INTERFERENCE FILTERS FOR TEMPERATURE SENSING, LIQUID DETECTION AND MODE-LOCKED LASER APPLICATIONS

YANG YAOXIAN

FACULTY OF ENGINEERING
UNIVERSITI MALAYA
KUALA LUMPUR

2024

INTERFERENCE FILTERS FOR TEMPERATURE SENSING, LIQUID DETECTION AND MODE-LOCKED LASER APPLICATIONS

YANG YAOXIAN

DISSERTATION SUBMITTED IN FULFILLMENT OF THE REQUIREMENTS FOR THE DEGREE OF MASTER OF ENGINEERING SCIENCE

FACULTY OF ENGINEERING
UNIVERSITI MALAYA
KUALA LUMPUR

2024

UNIVERSITI MALAYA

ORIGINAL LITERARY WORK DECLARATION

Name of Candidate: Yang Yaoxian

Matric No: S2142180/1

Name of Degree: Master of Engineering Science

Title of Project Paper/Research Report/Dissertation/Thesis ("this Work"):

Interference Filters for Temperature Sensing, Liquid Detection and Mode-Locked Laser Applications

Field of Study: Engineering And Engineering Trades (Electronics And Automation)

I do solemnly and sincerely declare that:

(1) I am the sole author/writer of this Work;
(2) This Work is original;
(3) Any use of any work in which copyright exists was done by way of fair dealing and for permitted purposes and any excerpt or extract from, or reference to or reproduction of any copyright work has been disclosed expressly and sufficiently and the title of the Work and its authorship have been acknowledged in this Work;
(4) I do not have any actual knowledge nor do I ought reasonably to know that the making of this work constitutes an infringement of any copyright work;
(5) I hereby assign all and every rights in the copyright to this Work to the Universiti Malaya ("UM"), who henceforth shall be owner of the copyright in this Work and that any reproduction or use in any form or by any means whatsoever is prohibited without the written consent of UM having been first had and obtained;
(6) I am fully aware that if in the course of making this Work I have infringed any copyright whether intentionally or otherwise, I may be subject to legal action or any other action as may be determined by UM.

Candidate's Signature Date: 28 June 2024

Subscribed and solemnly declared before,

Witness's Signature Date: 28 June 2024

Name:

Designation:

INTERFERENCE FILTERS FOR TEMPERATURE SENSING, LIQUID DETECTION AND MODE-LOCKED LASER APPLICATIONS

ABSTRACT

Interference filter, also known as a thin film filter or dielectric filter, is an optical device that selectively transmits or reflects specific wavelengths of light according to the principle of interference. As an advanced optical transmission and sensing technology, optical fiber technology plays a key role in communication, sensing, medical, industrial and scientific fields. This paper aims to discuss the principles and diversified applications of some of these technologies. One of the most widely utilised approaches in substance detection is optical sensor detection. Through the interaction of the sample on the wave characteristics of light, the absorption spectrum, scattering spectrum and transmission spectrum are analyzed to determine the properties of the material composition. This detection method is not only simple to operate, but also has the advantages of high accuracy, non-contact, fast detection speed and high sensitivity. The researchers found that based on the fiber conduction characteristics and the interaction between light and matter, the light signal results can be analyzed to determine the material composition and other properties of the test sample. In this paper, the sensitivity of microfiber sensing technology and Singlemode-Multimode-Singlemode (SMS) fiber structure based on step large-core multimode fiber in temperature and refractive index sensing is discussed. The microfiber ring resonator (MRR) structure based on flame heating conical stretching technology has great research potential in the field of sensing. In this paper, a MRR sensor with a ring diameter of about 400μm and an optical fiber diameter of about 2μm has been successfully prepared. At the same time, the standard single-mode fiber (SMF-28) and the advanced multimode fiber (MMF-S105/125-22A) are fused together, and the SP-

DSMSFR sensor is fabricated by side-grinding D-shape grinding in the centre of the multi-mode fiber. The experiments of temperature change, different solution and glycerin solution were carried out on the two sensors respectively. Compared with the experimental results, both sensors have good detection performance and have the potential to be used as solution detectors. In addition, SMS fiber is integrated into the ring cavity of an erbium-doped fiber laser (EDFL) as a saturable absorber (SA). A stable mode-locked pulse laser is obtained.

Keywords: Micro-fiber ring resonator, Temperature, Glycerin Solution, SMS fiber, Mode-locked laser.

PENAPIS GANGGUAN OPTIK UNTUK APLIKASI PENDERIAAN SUHU, PENGESANAN CECAIR DAN LASER DALAM OPERASI MODE-LOCKED

ABSTRAK

Penapis gangguan, juga dikenali sebagai penapis filem nipis atau penapis dielektrik, ialah peranti optik yang secara selektif menghantar atau memantulkan panjang gelombang cahaya tertentu mengikut prinsip gangguan. Sebagai teknologi transmisi dan penderiaan optik termaju, teknologi gentian optik memainkan peranan penting dalam bidang komunikasi, penderiaan, perubatan, perindustrian dan saintifik. Kertas kerja ini bertujuan untuk membincangkan prinsip dan aplikasi kepelbagaian beberapa teknologi ini. Pengesanan sensor optik adalah salah satu kaedah yang paling biasa digunakan dalam pengesanan bahan. Melalui interaksi sampel pada ciri gelombang cahaya, spektrum serapan, spektrum serakan dan spektrum penghantaran dianalisis untuk menentukan sifat komposisi bahan. Kaedah pengesanan ini bukan sahaja mudah untuk dikendalikan, tetapi juga mempunyai kelebihan ketepatan yang tinggi, tidak bersentuhan, kelajuan pengesanan pantas dan kepekaan yang tinggi. Para penyelidik mendapati bahawa berdasarkan ciri pengaliran gentian dan interaksi antara cahaya dan jirim, keputusan isyarat cahaya boleh dianalisis untuk menentukan komposisi bahan dan sifat lain sampel ujian. Dalam kertas ini, kepekaan teknologi penderiaan gentian mikro dan struktur gentian mod tunggal berbilang mod tunggal berdasarkan gentian berbilang mod teras besar langkah dalam suhu dan penderiaan indeks biasan dibincangkan. Struktur mikro-fiber ring resonator (MRR) berdasarkan teknologi regangan kon pemanasan api mempunyai potensi penyelidikan yang besar dalam bidang penderiaan. Dalam kertas ini, sensor MRR dengan diameter cincin kira-kira 400μm dan diameter gentian optik kira-kira 2μm telah berjaya disediakan. Pada masa yang sama, gentian mod tunggal standard (SMF-28) dan gentian berbilang mod lanjutan (MMF-S105/125-22A) dicantumkan

bersama, dan sensor SP-DSMSFR direka oleh pengisaran sisi D- pengisaran bentuk di tengah gentian pelbagai mod. Eksperimen perubahan suhu, larutan berbeza dan larutan gliserol telah dijalankan pada kedua-dua penderia tersebut. Berbanding dengan keputusan eksperimen, kedua-dua sensor mempunyai prestasi pengesanan yang baik dan berpotensi untuk digunakan sebagai pengesan penyelesaian. Di samping itu, gentian SMS disepadukan ke dalam rongga gelang laser gentian doped erbium (EDFL) sebagai SA. Laser nadi modelock yang stabil diperolehi.

Keywords: Resonator cincin gentian mikro, Suhu, Penyelesaian Gliserin, gentian SMS, laser Mode-locked.

TABLE OF CONTENTS

LIST OF TABLES

LIST OF FIGURES

LIST OF SYMBOLS AND ABBREVIATIONS

MRR	:	Micro-fiber Ring Resonator
SMS	:	Sing-mode Multi-mode Single-mode
SP-DSMSF	:	Side-Polished D-shaped SMS Fiber
HPLC	:	High-Performance Liquid Chromatography
GC	:	Gas Chromatography
MS	:	Mass Spectrometry
MF	:	Micro-Fiber
DEG	:	Diethylene Glycol
GCEs	:	Glassy Carbon Electrodes
SPR	:	Surface Plasmon Resonance
SMF	:	Single-Mode Fiber
MMF	:	Multi-Mode Fiber
SMSF	:	Singmode-Multimode-Singlemode Fiber
RI	:	Refractive Index
RIU	:	Refractive Index Unit
FSR	:	Free Spectral Range
DFBL	:	Distributed Feedback Laser
DBRL	:	Distributed Bragg Reflector Laser
EDFL	:	Erbium-Doped Fiber Laser
SIMF	:	Step-Index Multimode Fiber
MMI	:	Multi-Mode Interference
OFIs	:	Optical Fiber Interferometers
SML	:	Single Mode Light
ASE	:	Amplified Spontaneous Emission

OSA	:	Optical Spectrum Analysis
OPM	:	Optical Power Meter
SA	:	Saturable Absorber
G/W	:	Glycerin/Water
WDM	:	Wavelength Division Multiplexer
OC	:	Optical Coupler
PVA	:	PolyVinyl Alcohol
PRR	:	Pulse Repetition Rate
PC	:	Polarization Controller
NOLM	:	Nonlinear Optical Loop Mirror
NPR	:	Nonlinear Polarization Rotation
NALM	:	Nonlinear Amplifying Loop Mirror
FBG	:	Fiber Bragg Gratings
FWHM	:	Full Width Half Maximum
RFSA	:	Radio Frequency Spectrum Analyzer

CHAPTER 1: INTRODUCTION

1.1 Background

An optical fiber is a flexible strand made of either glass or plastic, capable of transmitting light from one end to the other. These fibers play a crucial role in fiber-optic communications, offering advantages such as extended transmission distances and higher bandwidths compared to traditional electrical cables (Born & Wolf, 2013). The fundamental principle governing light wave propagation in optical fibers is total internal reflection. In addition to their role as a transmission medium in telecommunications, optical fibers can serve as versatile sensors for measuring various parameters, including strain, temperature, and pressure. These sensors may detect changes in light intensity, phase, polarisation, wavelength, or period of transit by modifying the fiber, enabling a wide range of applications (Rajan, 2017). Optical fiber sensing constitutes a significant research field within fiber optics. In this context, the optical fiber medium is employed to monitor alterations in optical propagation features caused by environmental changes, encompassing physical, chemical, or biological factors as the light propagates through the fiber (Fang et al., 2012).

Glycerin is a colourless, odourless and viscous oily liquid that is easily soluble in water and can be miscible with many organic solvents due to its special chemical structure (Holloway et al., 2010). In general, glycerin solution itself is safe, non-toxic, and harmless. Because of these characteristics and high safety properties, glycerin has been widely used in industry. For instance, it can be used as a sweetener and preservative in the food industry because of its sweet taste and moisture absorption, respectively (Eitenmiller & Lee, 2004). In the pharmaceutical industry, glycerin is used as an excipient of drugs as well as a solvent and lubricant (Rowe et al., 2009). Glycerin is widely used in cosmetics and care products because of its moisturizing characteristics (Jungermann &

Sonntag, 2018). Because of this, the potential hazards of glycerin are often overlooked (Williams et al., 2013). Under special circumstances, people may unconsciously ingestion of excessive or high concentration of glycerin solution and harm their own health (Kienhuis et al., 2015), for example, excessive or long-term use of laxatives containing glycerin will cause diarrhoea, abdominal cramps, dehydration and other diseases; Long-term exposure to high concentration glycerin vapor or accidental inhalation of atomized glycerin solution will cause respiratory diseases such as difficult breathing and cough (Kienhuis et al., 2015). In addition, because glycerin is not only often used as an organic solvent and easy to enter the skin, special attention should be paid to the treatment of non-pure glycerin solution to avoid direct contact with the skin to cause toxic substances to enter the body and affect health (Sedghi et al., 2022).

Because of the wide application of glycerin and the inevitable safety risks, the detection of glycerin solution has become an important part of the quality control of glycerin products, compliance with regulations and process optimization. At present, the mainstream testing technologies used in industrial sites are mainly the following four: High Performance Liquid Chromatography (HPLC), Spectrophotometry, Gas Chromatography (GC), Refractometry. HPLC is one of the powerful analytical technologies widely used in the field of substance detection. Based on the liquid chromatography principle, it employs a high-pressure pump to propel the liquid mobile phase through a column containing a fixed phase, allowing various substances to interact to varying degrees after the fixed phase is removed and subsequently separate (Dong, 2006; Snyder et al., 2010). The GC principle is comparable to that of HPLC, but it relies on the interaction between the mobile phase of the gas and the fixed phase to complete the detection and quantitative separation of compounds (Al-Bukhaiti et al., 2017; Niessen, 2006). The glycerin solution detection method based on HPLC and GC technology is

highly sensitive, highly selective and can be used for batch detection, but the cost is high, so it is only suitable for large-scale factories (Ahuja, 2000).

Refractometry is based on the principle that the deflection phenomenon is caused by different propagation speeds in different media during the process of light propagation. The relative properties of the measured material are measured by calculating the deflection degree between the expected optical path and the actual optical path (Jha et al., 2009; Skoog et al., 2013). Spectrophotometry is also based on the principle of correlation optics, which uses the Beer-Lambert Law to correlate analyte concentration with light intensity absorption (Skoog et al., 2017). The glycerin solution detection method based on Refractometry and Spectrophotometry technology has the characteristics of low cost and efficiency, but it cannot achieve large-scale detection, so it is suitable for laboratory. Therefore, at present, researchers in the field of glycerin solution sensors mainly focus on the development of low-cost, efficient, high sensitivity and easy to carry glycerin solution sensors (Gaussoin et al., 2013; Higashihara & Ueda, 2015).

In the application of optical fiber, another important technology is the optical fiber filter. Like the electronic filter, the main function of the optical fiber filter is to filter out the noise or useless signals in the optical signal, retain the necessary useful signals, such as mode selection, frequency selection and obtaining narrow linewidth laser light source, etc., is an important passive device necessary for the development of broadband fiber communication at present and in the future. The optical filter has two main aspects according to the application: First, the optical filter applied to space optical communication can be divided into absorption type, interference type, birefringent type (Lyot type) and atomic resonance type (Gagliardi & Karp, 1997); Second, it is an optical filter applied to narrow the spectral width of the laser, such as the external cavity feedback semiconductor laser, the external cavity grating half-conductor laser and DFBL, DBRL,

etc., developed in the early 1980s (Agrawal, 1984; Lam & Garside, 1981). At present, fiber filters mainly include fiber single loop, fiber multiple loops, fiber loop with amplifier, fiber F-P cavity, fiber grating and semiconductor fiber ring cavity.

This thesis explores the deployment of two types of interference filter: microfiber ring resonator and single-mode-multimode-single-mode fibre (SMS) structure for sensor and laser applications.

1.2 Research Motivation

Optical sensors are one of the most used means of substance detection. Through the interaction of the sample on the wave characteristics of light, the absorption, scattering and transmission spectra are analyzed to judge the properties of the material composition (Girault et al., 2015; Lou et al., 2014). This detection method is not only simple to operate, but also has high accuracy. In addition, due to its non-contact, rapid detection, high sensitivity and other advantages, the field of optical sensors has been concerned (Xu & Brambilla, 2007). As a common optical material, the researchers found that based on its conduction characteristics and the interaction between light and matter, the optical signal results can be analyzed to determine the material composition and other properties of the test sample. At present, microfiber sensors in fiber-based sensing technologies have attracted much attention because of their advantages of optical sensors, smaller size and easier integration (Xu et al., 2014).

Microfiber is a type of optical waveguide made of glass or other transparent material, usually a few micrometers in diameter. Compared with traditional fiber, microfiber has the benefits of low loss and high sensitivity to changes in the surrounding environment. They are also more adaptable and manageable, making them appropriate for a broader

range of applications. Microfiber ring resonator (MRR) is an optical resonator made of a fiber loop with a diameter of several microns. It consists of straight sections of fibers bent into a ring, the ends of which are joined together to form a closed loop. The light can be coupled to the fiber through the conical fiber or the waveguide, and propagates around the ring, and due to the nonlinear optics of the micro-fiber shaped resonator, the characteristics of anti-interference, measurement stability, etc. (Yipeng et al., 2015).

In recent years, the multi-mode interference (MMI) effect in multi-mode fiber (MMF) has attracted extensive attention in the sensing field (Guzmán-Sepúlveda et al., 2021; Lee & Kim, 2006). SMS fiber structure is one of the most widely used fiber structures in the study of mode interference in multimode fibers (Silva et al., 2012; Wang & Farrell, 2006). The SMSF structure is associated with the usage of a SMF as the import end of the propagation light into the MMF, and subsequently as the export fiber from the MMF output end of the SMF. In general, the specifications of the SMF utilised by the importing fiber and the exporting fiber are the same, and the MMF has a large core diameter that can excite several modes. At present, some people have applied various characteristics of SMS to realize the monitoring of many common parameters such as displacement sensing (Mehta et al., 2003; Ribeiro et al., 2004), temperature sensing (Fuentes-Fuentes et al., 2015), and micro-bending sensing (Donlagi & Culshaw, 2000), and some scientists have proposed a bandpass filter based on SMS (Mohammed et al., 2006). In addition, its special transmission characteristics make it an ideal platform for mode-locked EDFL (Luo et al., 2023; Yang et al., 2023). The design of mode-locked EDFL based on the SMS fiber structure has several advantages, such as its unique nonlinear characteristics and optical mode coupling effect, which facilitate the formation and regulation of pulses (Wang et al., 2019). Besides, the special layout of the SMSF structure can also effectively inhibit

multi-mode excitation and provide optical pumping conditions, helping to enhance the performance and stability of the laser (Fu et al., 2015; Wang et al., 2008a).

1.3 Problem statement

Microfiber ring resonators (MRRs) are crucial in silicon photonics for efficiently guiding light within extremely small spaces. These optical waveguides loop light back on themselves to achieve resonance at specific wavelengths. While MRRs are currently integral to optical communication systems, offering high nonlinear effects and all-fiber structures for signal processing and pulse shaping, they also hold promise for sensing applications, particularly in substance detection. However, conventional MRR fabrication using silicon photonics or integrated waveguide platforms is complex and costly. Similarly, the fabrication of inline Mach Zehnder interferometers requires sophisticated integrated photonics platforms. This study investigates a low-cost approach to fabricate MRRs using microfiber technology based on a flame brushing technique. A single-mode-multimode-single-mode (SMS) fiber structure created through fusion splicing is used as an inline Mach Zehnder interferometer.

1.4 Research Objectives

This thesis aims to develop the MRR and SMS device for temperature sensing, liquid detection and mode-locked laser applications. The following aims will guide the investigation.

- To fabricate MRR and SMS device using a flame brushing technique and fusion splicing, respectively and characterize them.

- To demonstrate two temperature and glycerin sensors using MRR and SMS device respectively, which based on the resonance wavelength shift and intensity modulation as sensing sensitivity.
- To demonstrate an erbium-doped fiber mode-locked pulse generation using a SMS structure as an artificial saturable absorber.

1.5 Thesis Overview

This thesis mainly introduces two kinds of optical resonators: MRR and SMS for both sensor and laser applications. It comprises six chapters providing an experimental study on MRR for sensing applications and SMS for both sensing and laser applications. The current chapter briefly introduces the optical fiber resonator and sensors, including this thesis's motivation and objectives. The second chapter provides a thorough literature review on the two kinds of optical fiber interference filters. Chapter 3 reports on the fabrication and characterization of the MRR and SMS filters. In Chapter 4, the temperature and glycerin sensors are reported using MRR and SMS device. The application of SMS in generating mode-locked pulses is presented in Chapter 5. The finding of this work is concluded in Chapter 6.

CHAPTER 2: LITERATURE REVIEW

2.1 Introduction

Glycerin as a widely used industrial product, its own has a variety of advantages, can be used as medicine, can be used as an organic solvent, can also be used as a cosmetic additive (Poblete-Castro et al., 2020). But it is precisely because of these characteristics that the potential danger of glycerin solution has been ignored by people. For example, glycerin itself does not have any toxicity, but there will be diethylene glycol (DEG) mixed in the reproduction process, DEG is a highly toxic substance, so the detection of glycerin solution is very necessary. Accurate detection and quantification of glycerin is therefore essential for quality control, regulatory compliance, and ensuring consumer safety (Holloway et al., 2010; Luo et al., 2014).

2.2 Types of Glycerin Sensors

At present, the technical means for glycerin detection in production and life are mainly: HPLC, GC, Refractometry and Spectrophotometry. The working principle of HPLC is actually to use the filling column to separate the passing sample mixture into separate components with the help of different interactions between different substances and the filling column, and to classify and quantify the results according to their retention time and peak height (Ahuja & Dong, 2005; Pragst, 2008). The basic working principle of GC is exactly the same as that of HPLC, GC is the result of separating and quantifying the test sample (gas) through a coated capillary column (stationary phase), and therefore the detection of volatile or low boiling point substances (Grob & Barry, 2004; Watson, 2020). These two detections mean have high sensitivity, high selectivity, and relatively mature technical products, but also have high detection costs, more complex instrument structure

is not convenient to carry and other problems. At present, most commercial glycerin sensors can be integrated and lightweight and easy to carry under the premise of high sensitivity (Snyder et al., 2011).

2.2.1 Electrochemical Sensors

An electrochemical detector is a type of analytical instrument that detects and quantifies an analyte in a sample using electrochemical principles, specifically the electrical response generated by the interaction of an analyte and an electrochemical system (typically consisting of electrodes and electrolytes). Chen et al. developed a non-enzymatic electrochemical approach with PtRu-modified-screen-printed sideband ultra-micron electrode for the selective and sensitive detection of glycerin in order to build a selective and sensitive approach to the determination of glycerin. This method combined the two phases of sample preparation and detection into a single step. The approach eliminates practically all interferences in the solution phase, resulting in a very selective glycerin analysis (Chen et al., 2015). Arevalo et al. performed an electrochemical oxidation of GLY on a multi-walled carbon nanotube/pectin composite material using a glassy carbon electrode modified with copper oxide nanoparticles. The electrochemical sensor is capable of detecting glycerin in biodiesel samples and has good performance, stability, reproducibility, and repeatability, as well as a good detection limit and linear concentration range (Arévalo et al., 2017). Li et al. attempted a method for the direct electrochemical detection of glycerin using hot annealed gold nanoparticles. The method is simple and sensitive, and can be accurately detected in glycerin samples, which provides a new way for the study of electrochemical reaction in microenvironment and the construction of alcohol sensors (N. Li et al., 2014). Motia et al. developed a portable electrochemical glycerin detection sensor using Au-SPE coated polyacrylamide and

AuNPs matrix. The sensor offers high sensitivity, good selectivity, a quick reaction time, good reproducibility, and stable operation and storage (Motia et al., 2020). Paiva et al. used cyclic voltammetry to estimate glycerin electrochemically and built an electrode for glycerin determination in biodiesel out of reduced graphene oxide and core-shell gold/palladium nanoparticles modified glassy carbon electrodes (GCEs). The approach has a number of benefits of being quick, sensitive, low cost, stable, and requiring less reagent. It is an excellent method for analysing glycerin in biodiesel (Paiva et al., 2021).

2.2.2 Enzymatic Biosensors

Enzyme biosensors utilize specific enzymes, such as glycerin kinase, glycerin dehydrogenase, or lipase, to selectively react with glycerin and produce a measurable signal. Ali Eftekhari used potassium ferricyanide as the medium of biosensing reaction and fixed glycerin dehydrogenase in polyaniline film to prepare the enzyme modified electrode, thus producing a glycerin detection sensor with good stability and selectivity (Eftekhari & Chemical, 2001). de Souza et al. compared two enzymatic methods for the determination of glycerin content based on two coupling activities (glycerin quinase and glycerin-3-phosphate oxidase), amperometry method and colorimetric method, and applied the two methods to the determination of glycerin in beverages, and the results showed that the two methods had a good correlation (de Souza et al., 2013).

2.3 Optical Sensors

Optical sensors have unique advantages in solution detection. Optical sensors are very sensitive to changes in concentration (Yu et al., 2014). By measuring properties such as absorption, scattering, transmission or emission of light, precise detection of the

concentration of target substances in solution can be achieved (Forouzeshfard et al., 2021). Optical sensors are usually non-contact and do not require direct contact of the sensor with the solution. This non-destructive detection method avoids contamination or damage to the sample, while providing the ability to continuously monitor without interrupting the normal flow of the solution (Su et al., 2021). Optical sensors can monitor concentration changes in solutions in a real-time manner. With fast response and high sampling rate, the optical sensor can provide instant measurement results, allowing the operator to keep abreast of the changing trend of the concentration of substances in the solution (Taya et al., 2022). Optical sensors can measure multiple parameters simultaneously. Simultaneous detection of multiple species concentrations can be achieved by selecting appropriate optical detection techniques and sensor configurations. This multi-parameter detection capability makes optical sensors very useful in complex solution analysis and real-time monitoring (Wan et al., 2021). Optical sensors can enhance their selectivity for specific substances by choosing appropriate optical probes or absorbers. By designing and optimizing the characteristics of target substances, optical sensors can achieve highly selective detection of specific solution components and avoid interference with other interfering substances (Liu et al., 2021).

De et al. created a low-cost optical detector based on porous silicon nanotechnology, which they used to measure and evaluate pesticide levels in water and humic acid solutions. Even at low concentrations of 1 Vol, a clear light signal change can be recorded. The consequence is triggered by capillary penetration of liquid into the pores, and it enables modifications to the RI of liquid solutions to be detected down to 0.0002 (De Stefano et al., 2005). Su et al. constructed an easy-to-understand fiber optic sensor with two photodetectors, three couplers, a single diode optical laser as an energy source and two detecting fiber ends with protective cladding. Different concentrations of seawater

and sugar-containing solutions were measured. The measured data fit well with the linear equation, with R^2 greater than 0.995 (Su & Huang, 2007). Canning et al. developed and validated a fiber-optic biosensor that utilised surface plasmon resonance (SPR). The sensor's SPR spectra for varied concentrations of glucose solutions were recorded. When glucose and glucose oxidase come into contact, a chemical reaction occurs, changing the RI of the fixed GOx film and shifting the resonance wavelength (Canning et al., 2012). Jin et al. constructed an exclusive solution percentage detector based on the SMF-EMMF-FBG structure. The sensing capabilities of fiber gratings in relation to solution concentration were investigated. Using the wavelength difference between the high mode and the essential mode, the experiment was able to detect and detect four different types of solutions. The high order mode of the etched multimode fiber is more susceptible to the underlying RI than the standard mode (Jin, 2013).

The following Table 2.1 lists some of the work on liquid refractive index sensing in the last five years.

Table 2.1: Previous Work on Liquid Refractive Index Sensing

Type of Sensor	Structure	Liquid	Sensitivity	Ref.
Optical Fiber Sensor	D-shaped SMS fiber Structure	Glycerin Solution	18.7 RIU^{-1}	(Mu et al., 2020)
Biosensor	1D TPC consisting of crown glass, silicon nitride and titanium dioxide.	water concentration in ethanol	144.369 nm/RIU	(Taya et al., 2022)
Optical chemical sensor	A optical chemical sensor based PCF in the terahertz spectral region	water concentration in ethanol	96.39 nm/RIU	(Hossain et al., 2021)
SPR Sensor	A multi-channel surface plasmon resonance (SPR) sensor, employing space division multiplexing (SDM) technology	Glycerin Solution	2655 nm/RIU (Average)	(Feng et al., 2023)
Biosensor	A polymethyl methacrylate (PMMA) fiber RI sensor based on SPR	Glycerin Solution	3328.1 nm/RIU	(Lv et al., 2021)

2.4 Microfiber

The unique features of microfibers, such as evanescent field beam confinement, tunability, beam confinement, and flexibility, make them ideal for physical sensing applications like as biological and RI sensors, SPR absorption spectroscopy, and blood oxygen monitoring (Chen et al., 2013). In consequence of the enormous evanescent field which propagates outside the MF, the MF is exceptionally sensitive to fluctuations in its external refractive index (Lim et al., 2012b). The RI of the unique material increases according to the power percentage of the light field propagating in the evanescent field. It has strong interactions with its surroundings and has good evanescent coupling

capabilities with metals, semiconductors, and substrates in other waveguides. According to the findings, the high intensity evanescent field can respond swiftly to the detection of water molecule content in the air (Chen et al., 2013).

The fact that MF possesses numerous surprising fluctuating optical and engineering stress qualities is apparent, as is the fact that it has a unique field, a field in which light propagates swiftly. In the evanescent field, fractional power expands outside the physical boundary of the non-significant radius MF. This function is required for light to enter the high Q-factor resonator.(G. J. O. F. T. Brambilla, 2010). MF additionally communicates substantially with other objects through the near field (Wu & Tong, 2013). It possesses excellent evanescent linking from the MF to other waveguides such as substrate (Coillet et al., 2010), semiconductor (Ding et al., 2009), planar waveguide and metal (Armani et al., 2003). This resulted in the development of numerous new optical devices, including sensor, resonator and laser (Jiang et al., 2006).

Furthermore, due to its small mass, changes in photon wave momentum generated by stress displacement owing to external changes or vibration mass are particularly sensitive to MF (Wu & Tong, 2013). This allows for the manufacturing of minimal optomechanical elements and gadgets (Le Kien et al., 2006). Traditionally, facilitates low-loss propagation of light when it encounters severe bends. As a consequence, MF might promote the fabrication of a micro gadget with more quick flexibility, smaller footprints , lower power consumption (Tong et al., 2004; Wu & Tong, 2013). In general, when producing MF, it is necessary to cut the appropriate length in a whole section of fiber, remove the external coating in the middle of the intercepted fiber, ensuring that the original diameter of the two ends of the fiber remains constant, and then stretch the exposed glass fiber in the middle until the desired result is obtained. This procedure can

assure that there will be no significant propagation loss in the subsequent optical fiber splicing.

Multiple approaches to generate MF have been established. The primary method is commonly referred to as a self-modulated taper drawing. It is a procedure that consists of two stages: to begin, the most traditional flame brushing approach was utilised to stretch the diameter of the SMF removing coating part to several m. The MF is then treated as two distinct components, with one end of the fiber wrapped around a heated tiny sapphire rod to stretch the MF to a diameter of nm. It should be noted that during the stretching process, the fiber should not come into direct contact with the flame used to heat the sapphire, and the sapphire tip should be heated with a flame at a certain distance, so that the high temperature can be concentrated in a closed container to obtain a stable and uniform heating temperature. (G. J. J. o. O. Brambilla, 2010). Without considering the complexity of processing cost and operation technology, the radius of MF produced by this process can reach a minimum of 50nm (Tong et al., 2005).

The second way of acquiring MF differs significantly from the first. Because we all know that the majority of optical fiber cores on the market are composed of glass, you have the option of directly extracting the glass material from which the fiber cores are constructed. To generate a radius of MF in the micron range, a very small sapphire rod heated by high temperature blue fire and glass material were swiftly contacted and separated. The basic idea behind this process is to utilise a high-degree hot rod to swiftly contact and soften the glass material, causing it to partially stick to the rod surface, and then quickly exit the MF moulding by utilising temperature fluctuations.(G. J. J. o. O. Brambilla, 2010). The advantages of this strategy are more obvious, namely flexibility and low equipment costs. The similar drawback exists in this opinion, in that obtaining

the perfect radius of MF necessitates numerous experiments and some luck (Tong et al., 2006).

The third method depends on the flame brushing approach that had previously been employed to generate a fiber connector (Bilodeau et al., 1988). It is accomplished by circulating a tiny blue hot flame across a small area under a stretched optical fiber repeatedly. The optical fiber ends are fixed in two movable drawing tables, and both the flame moving and optical fiber drawing tables are controlled by the same electronic central controller. By accurately controlling the flame movement, an incredibly accurate MF may be generated (Birks & Li, 1992). It is geared towards manufacturing microfibers with diameters less than 30 nm (Brambilla et al., 2006). Meanwhile, this method makes it possible to easily connect the MF ends to other instruments that is especially essential in applications that exist in reality with difficulties with connectivity. The MF was manufactured in this study utilising a flame brushing approach and a homemade fiber tapering machine, as shown in Figure 2.1. The manufacturing equipment is supplied with electricity by an oxy-butane burner, a microcontroller, and stepper motors.

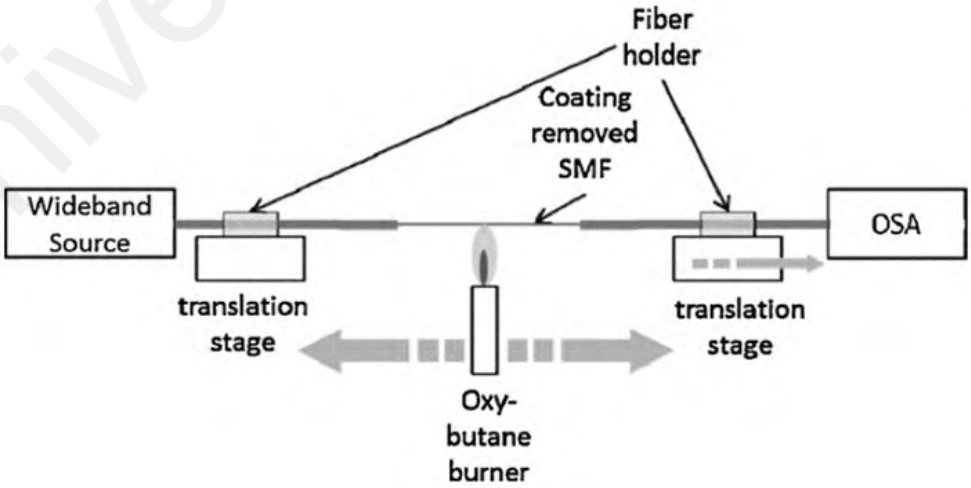

Figure 2.1: Experimental setup for flame brushing technique to fabricate MF (Harun et al., 2013)

The above three methods are compared and summarized in the Table 2.2.

Table 2.2: Comparison of the three fabrication methods for the microfiber

Type of Methods	Result	Comments
Two-Step Stretching Method	The minimum diameter of the microfiber is 50nm.	The process cost is high and the operation is complicated.
Self-Modulated Drawing Force Method	The minimum diameter of the microfiber is 20 nm with the uniformity up to 0.1%.	The stability and repeatability are difficult to guarantee for the manual preparation methods due to the random factor of human and the airflow disturbances of external environment in the drawing process.
Flame Brushing Technique	The minimum diameter of the microfiber is 30nm.	This method can not only ensure the accuracy of the finished product, but also greatly simplify the difficulty of operation and reduce the process cost.

Aside from the tapering technique, heat sources are also significant when producing high-quality MF. Four heat sources are usually employed throughout the tapering process, such as flame (Kieu & Mansuripur, 2006), fusion splicer (Corres et al., 2006), CO2 laser beam (Kakarantzas et al., 2001) and micro furnace (Corres et al., 2006). MF can be formed into a variety of shapes and features by altering tensile parameters such as heating zone width, contact temperature, and tensile speed. As illustrated in Figure 2.2, the high temperature blue flame generated by the gas formed by mixing methane gas and oxygen after ignition is the most often employed heat source for heating the optical fiber core in terms of both cost and outcome. Because the central controller controls the entire process, the radius of the optical fiber core will progressively shorten and the length of the fiber core will gradually lengthen at the specified drawing speed. This process is repeated two or three times until the necessary length or radius is attained by the repetitive movement

of the flame and the slow outward movement of the drawing table. The core of the created MF changes from fine to thick at both ends, which is known as the "biconical" fiber taper (Wu & Tong, 2013). The waveguide features of MF can be determined during the stretching process using the loss of propagation in OPM and the MMI spectral image in OSA (Boucouvalas & Georgiou, 1985). The negative aspects associated with employing the flame-heating method include unpredictable instability of the methane gas and oxygen throughout the burning process. As a result, CO2 lasers have been exposed to address this problem (Wu & Tong, 2013). When the fiber diameter reaches a particular value, the stretching process is automatically stopped by direct laser heating (Bohren & Huffman, 2008; Dimmick et al., 1999). Another method is artificially heated taper drawing, which enables for greater flexibility in drawing MF. By accurately controlling the temperature distribution, this approach allows the MF to be shaped into various geometries (Coillet et al., 2010; Wu & Tong, 2013).

Figure 2.2: Fabrication technique of the MF using flame heated source (Wu & Tong, 2013)

2.5 Singlemode-Multimode-Singlemode Fiber (SMSF) Structure

In the area of detecting, the mode interference influence in MMF has recently gotten a lot of interest from researchers in the field (Lee & Kim, 2006). The mode interference

condition originally emerged in planar waveguides and has since been applied to the fabrication of photonic integrated circuits and a wide range of operational optical equipment (L. B. Soldano & E. C. J. J. o. l. t. Pennings, 1995), including beam splitters, Mach-Zehnder converters (Zhao et al., 2021), modulators and balanced coherent receivers. As the initial signal transmission fiber, multimode fiber has the characteristics of multiple conduction modes and sensitive response to external interference. An acceptable detecting system can be established by employing the interaction between the output light and the nearby atmosphere as it propagates through the MMF. The primary mechanism of these sensors relies on the MMI effect in the MMF, which causes the pattern of distribution of the MMF's longitudinal (fiber transmission direction) optical field to change with distance on a periodic basis (Irawati et al., 2019). The incident light is emitted to the MMF with a certain form of incident light field, and when it is transmitted along the multimode fiber for a certain distance, the optical field distribution of the multimode fiber will appear at this position and the distribution of the incident light field is almost the same, that is, the so-called self-focusing effect appears (X. Wang et al., 2017). MMF has been explored and employed in detection, filtering, and other domains as the consequence of the investigation of mode interference effect in MMF.

Since the publication of an article by Lucas et al in 1995 (Agrawal, 1984), which effectively and in detail clarified the mode interference effect in MMFs, and carried out detailed calculation and analysis on significant hypotheses such as mode interference effect, propagation field change, and self-image condition in MMFs, the academic field has once again given consideration to the mode interference effect in MMFs. Lay the groundwork for the establishment and growth of SMS. The paper also proposed the idea of making optical couplers using the mode interference effect in MMF, which became the first application based on the MMI effect in fiber in recent years. Compared with

directional couplers, diffraction star couplers and other traditional couplers, this coupler has many advantages, such as polarization immunity, wavelength multiplexing, excellent performance, etc., and has been widely concerned. In 1997, Denis et al. first proposed the concept of sensing with SMS (Đonlagić & Završnik, 1997). In his article, he mentioned the use of SMS fiber optic structure to achieve micro-bending sensing, which exceeds the sensitivity of traditional micro-bending sensors by 6 times. Since that, Denis et al. continued their SMS micro-bending monitoring research, thoroughly analysing the micro-bending loss of MMF and constructing an SMS-based distributed and quasi-distributed micro-bending detecting system. Due to the fact that SMS transmits by employing SMF, the system considerably lowers transmission loss caused by MMF and employs SMS's selective transmission properties to efficiently manage the series interference effect in classical micro-bending sensors. Considering SMS transmission properties are particularly sensitive to changes in the length of MMF sections, the researchers discovered that the SMSF structure can potentially be employed for measuring variations in small quantities of displacement, giving birth to the SMSF strain detecting technique. Alok et al. suggested a modest displacement sensing technique based on SMS during the turn of the century (Mehta et al., 2003). They proposed using a reflecting SMSF structure, in which the same SMF was employed as the inlet and outlet end of the MMF, to sense minor displacement changes via tracking the change in SMS output wavelength. Subsequently applying the hypothesis, Ribeiro et al. thoroughly examined the longitudinal strain response of the SMS propagation spectrum (Ribeiro et al., 2004). Waleed et al. issued a comparatively comprehensive explanation of mode interference in SMSF structure in 2004, which can be considered as an in-depth overview of previous SMSF structure investigation and evaluation, detailed investigation of the conditions required for mode interference to attain the self-focusing effect, and

recommended the application of the effect to make optical effective device-connector (Mohammed et al., 2004).

The mode interference impact of MMF in SMSF structure received significant concern in the field of fiber technology in recent years and has been intensively investigated in the implementation of monitoring and device manufacturing. Many critical factors in MMF, such as refractive index, core diameter, and core length, would be modified by changes in the surrounding temperature owing to the thermal optical effect and thermal expansion impact of fiber materials, implying that SMS transmission spectrum is also temperature sensitive (Tripathi et al., 2009). Based on this mechanism, Li et al. published relevant research results in 2006 (Li et al., 2006), using reflective SMSF structure to achieve high temperature measurement, which is another breakthrough in the application of SMS in the field of fiber sensing. Later, Li et al. published a paper discussing the temperature sensing performance of SMSF structures packaged (E. J. I. P. T. L. Li, 2007; E. J. O. l. Li, 2007). In the same year, Wang et al., of the Dublin Institute of Science and Technology in Ireland, proposed that because there are radiation modes in the MMF, which the optical transmission in the MMF will have mode leakage, and the transmitted light in the MMF will inevitably exchange information with the outside world (Wang & Farrell, 2006). When the environmental RI changes, the reflectivity of the leaked light will change, and the propagation spectrum of the SMSF structure will also shift. This paper proposes that the environmental refractive index can be sensed by monitoring the intensity change of SMS transmitted light and discusses the optimization scheme of using MMF with different core diameters to enhance the sensor sensitivity, and proposes the wavelength sensitivity of the surrounding RI. Although this paper only uses simulation analysis to show the theoretical feasibility of refractive index sensors, it is another breakthrough in the optical fiber sensing SMS, followed by a series of experimental

studies on SMS refractive index sensors in the scientific community. In 2007, He et al. conducted an experimental study on the SMS refractive index sensor (Shao et al., 2007). They increased the sensor sensitivity by tapering MMF, and engraved Bragg fiber grating at both ends of the SMS to achieve self-calibration refractive index measurement, which could not only overcome the instability brought by light source fluctuation and ambient temperature to the refractive index sensor. It can also realize dual detecting of RI and temperature. In the field of optical fiber communication, SMS structure is expected to achieve filtering function. Since SMS transmission spectral curves vary widely when multi-mode fibers with different parameters are used, it is possible to realize various filter functions. In addition to the bandpass filter discussed by Waleed et al., various functions such as band-stop filters and gain flatters are also expected to be introduced and applied under further research on SMS (Wang et al., 2008c).

2.5.1 Multimode Interference

The SMSF structure has been investigated applying the MMI concept of the MMF. SMS gains numerous unique traits as a result of this mode interference effect, such as self-focusing and spectrum response characteristics. These intrinsic properties of SMS can be used to make a variety of practical optical devices, which has triggered extensive research in recent years. The application of SMSF structure is mainly based on its spectral response characteristics. In this section, the output spectral response characteristics of SMS are derived from the light field distribution in the MMF.

Figure 2.3 illustrates the SMSF structure. The SMSF structure is constructed by splicing the SMF as the import end to the MMF with length L and width d, and then leading out with SMF as the export end. In general, the features of imported and exported

fiber are the same. In the mathematical investigation, we presuppose that the link between SMF and MMF is an ideal step structure, and that the SMF and MMF axes are totally consistent.

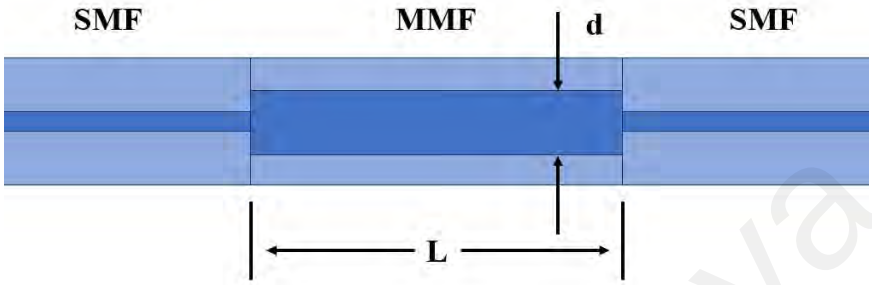

Figure 2.3: SMSF structure diagram

While the SML travelling in the imported fiber is incoming on the MMF in the SMSF configuration depicted in Figure 2.3, several independent eigenmodes get excited and transmitted in the MMF. When each mode propagates, they will interfere, resulting in a periodic arrangement of the light field in the MMF, which is commonly referred to as the mode interference effect in the MMF. Mode coupling occurs again when the transmission light in the MMF is incident on the MMF at the generating end, and this chain of actions causes the SML generated by SMS and the input SML to have distinct properties. When a wide-spectrum light source with homogeneous energy is used as the incoming light, the output light characteristics demonstrate that different wavelengths correlate to different light energies, which is reflected in the spectral qualities of the SMS structure.

2.5.2 Light Field Distribution in SMS Fiber Structure

The output spectra of SMSF structures are generated in three phases. To begin, the somewhat complex light field distribution in MMF is analysed and sorted out, and then

the correlation modulus with decisive energy in the transmission mode is calculated using inference. Finally, the output spectrum response characteristics are derived by examining the relationship between the primary modulus.

Under the on-line bias mode approximation, the light field distribution inside MMF can be applied to be a Gaussian beam at the inlet end of the SMF:

$$E_S(r) = e^{-\left(\frac{r}{\omega}\right)^2} e^{-i\beta_0 z} x \tag{2.1}$$

Where r is the radius of the SMF, and β_0 is the longitudinal (the direction of light transmission) propagation invariant of the single mode light. The half-height width ω of a Gaussian beam can be calculated by empirically mathematical equation:

$$\omega = \frac{a_0}{\sqrt{\ln 2}}(0.65 + 1.619V^{-1.5} + 2.879V^{-6}) \tag{2.2}$$

In the equation, $V = \frac{2\pi a_0}{\lambda}\sqrt{n_1^2 - n_2^2}$, where n_1 is the RI of the MMF core and n_2 is the RI of the MMF cladding.

Different modes of light get excited in the MMF and propagates in the fiber when the transmitted light travels through the SMF into the MMF. For specific parameters of MMF, the SML represented by equation(1) will excite a succession of corresponding optical propagation modes, including the guide mode restricted to propagation in the fiber and the radiation mode spilled outside the fiber, forming an orthogonal system. The light field at any location in the MMF can be described as the set of all guide modes, ignoring the radiation mode. The transmitted optical field of MMF can be represented in cylindrical coordinates as (Calvo & Lakshminarayanan, 2018):

$$E(r,\vartheta,z) = \sum_{\mu=-M}^{M} \sum_{v=1}^{N} \psi_{v,\mu}(r,\vartheta,z) \tag{2.3}$$

where, v and μ are the radial component and angular component coefficients, and N and $2M+1$ are the total number of radial component and angular component modes, respectively. $\psi_{v,\mu}(r,\theta,z)$ represents the field vector of each guide mode.

Solving Maxwell's equations for linear polarization modes in the MMF using the separated variable method, the expression of Watt $\psi_{v,\mu}(r,\theta,z)$ can be obtained (Okamoto, 2021):

$$\psi_{v,\mu}(r,\theta,z) = \begin{cases} c_{v,\mu} J_\mu\left(u_{v,\mu}\frac{r}{d}\right)\cos(\mu\vartheta)\, e^{-i\beta_{v,\mu}z} x & r \le d \\ d_{v,\mu} K_\mu\left(\omega_{v,\mu}\frac{r}{n}\right)\cos(\mu\vartheta)\, e^{-i\beta_{v,\mu}z} x & r > d \end{cases} \tag{2.4}$$

where, u, ω and β are the transverse propagation coefficients in the core, the transverse propagation coefficients in the cladding and the longitudinal propagation coefficients corresponding to the normalized modes respectively. d multi-mode fiber diameter, $c_{v,\mu}$ and $d_{v,\mu}$ indicate the field excitation coefficient. The excitation coefficient can be associated with the following equation:

$$d_{v,\mu} = \frac{J_\mu(u_{v,\mu})}{K_\mu(\omega_{v,\mu})} c_{,\mu} \tag{2.5}$$

The transverse propagation coefficient in equation (2.4) is defined as:

$$u_{v,\mu} = d\sqrt{k_0^2 n_1^2 - \beta_{v,\mu}^2} \tag{2.6}$$

$$\omega_{\nu,\mu} = d\sqrt{\beta_{\nu,\mu}^2 - k_0^2 n_2^2} \tag{2.7}$$

where k_0 is the vacuum wave number.

When $z = 0$, this formula represents the optical field distribution at the interface of the imported SMF and MMF, and the transmitted optical field satisfies the continuity under boundary conditions, which should have the same properties as the input field described in equation (2.1). By comparing equation (2.1) and equation (2.3), there is no angular component in the input optical field described by (2.1), which indicates that there should not be any angular component contribution in the optical field of the MMF at the interface. In this case, the excitation factor should be zero when $\mu \neq 0$. Thus, the multi-mode light field at the interface can be simplified as:

$$E_s(r,0) = \begin{cases} \sum_{v=1}^{N} c_{\nu,0} J_0\left(u_{\nu,0}\frac{v}{d}\right)x & r \leq d \\ \sum_{v=1}^{N} d_{\nu,0} K_0\left(\omega_{\nu,0}\frac{r}{d}\right)x & r > d \end{cases} \tag{2.8}$$

For the convenience of writing, the subscript of the azimuth component is removed from the subsequent derivation, and the transverse and longitudinal propagation coefficients are expressed as u_ν, ω_ν, β_ν respectively. The excitation coefficient is written as c_ν, d_ν.

2.5.3 SMS Fiber Structure Output Spectral Response

The light field features of SMS are primarily affected by a few key modes with the highest energy. After determining the moduli that compose the major energy of the light field, we may calculate the interference effect between these dominating moduli by derivation to get the SMSF structure's output spectrum response.

In the optical field identified by equation (3), the difference between the longitudinal propagation coefficients v_m and v_n of two arbitrary modes can be built as follows (Smith et al., 1974):

$$(\beta_{vm} - \beta_{vn}) = \frac{u_{vm}^2 - u_{vn}^2}{2kd^2 n_1} \tag{2.9}$$

where k is the wave number of light.

When the phase difference between two separate modes is an integer multiple of 2π, the propagated light will be coherently overlaid, with regard of the interference concept of light. The coherence conditions are:

$$(\beta_m - \beta_n)L = 2\pi N \tag{2.10}$$

Then the wavelength formula when interference occurs is:

$$\lambda = \frac{8(2N+1)n_1 \mathrm{d}^2}{(m-n)[2(m+n)-1]L} \quad (m > n) \tag{2.11}$$

where L is the length of the MMF and N is an invariant. d indicates the core diameter of the MMF, where n_1 is the core refractive index. It can be seen from the formula that the factors affecting the wavelength change include the core RI n_1 of the MMF, core diameter d and the length L of the MMF, all of which serve as the basic theoretical basis for studying the external influence characteristics of SMS.

It is easy to see that for different wavelengths of incident light, the position of mode interference is not the same, and its energy distribution in multi-mode fiber is also different. In this way, the output energy of incident light of different wavelengths after transmission through SMS will eventually be different. When broad spectrum light is used as the incident light source for SMS, the output spectrum will be a spectral curve

with multiple wavelengths matching to different energies, which is the spectral response features of the SMSF structure.

Assume the incident light source of SMS is a broad-spectrum light $s_0(\lambda)$. The incident light gets triggered into N conduction modes at the interface of the entering SMF and the MMF via the first mode coupling. The propagated light is transformed back into SML at the interface of the MMF and the outgoing SMF by the second mode coupling. The V conduction mode's output light intensity in the MMF linked to the generated fiber should be:

$$s_v(\lambda) = \eta_v^2 s_0(\lambda) \tag{2.12}$$

The output light intensity in the fiber is produced by multiplying the superposition of the amplitudes of each guide mode in the MMF by its complex conjugation, which corresponds to the optical concept:

$$s(\lambda) = \sum_{i=1}^{N} \eta_i^2 s_0(\lambda) + \sum_{i \neq j=1}^{N} \eta_i \eta_j s_0(\lambda) \cos(\Delta\varphi_{ij}) \tag{2.13}$$

where, the phase difference is $\Delta\varphi_{ij} = (\beta_i - \beta_j)L$.

CHAPTER 3: PREPARATION AND CHARACTESTICS OF INTERFERENCE FILTERS

3.1 Introduction

Optical fiber presents numerous distinctive advantages compared to alternative transmission media, encompassing its compact size, lightweight nature, low propagation loss, and inherent immunity to interference from electromagnetic fields. Originating with the introduction of low-loss optical silica fiber in the 1960s and subsequent fabrication in the 1970s, this technology has undergone a continuous evolution fuelled by research-driven innovations (Fang et al., 2012; Ippen et al.). Its primary emphasis has been on communication and detecting applications. An optical fiber is normally made up of a high RI core covered in a lower RI cladding area. The junction between the core and the cladding allows for 100% internal reflection, allowing light to pass through the optical fiber. When utilizing low-loss materials like silica, ultralow transmission loss becomes achievable, resulting in minimal attenuation of the fiber, approximately 0.2dB/km at 1550nm. The exceptional feature of ultralow transmission loss lies in its capacity to enable optical fiber utilization for remote and distributed sensing applications. This capability allows for the detection of environmental variations, such as temperature, acoustic signals, and strain, across expansive geographical regions. The realm of optical fiber sensors encompasses diverse types and structures, ranging from fiber gratings and SPR to the OFIs (Sahota et al., 2020a; W. Wang et al., 2017).

Multiple beams are often propagated down separate optical fibers, or optionally along distinct routes inside single optical fibers, in an OFI. When beams are combined rather than a single light source, each beam has its own independent propagation path. However, when they come into contact with one other and light particles clash, they interfere with each other. Because of this irregular interference, which is either positive or negative,

light waves fluctuate throughout a wide range of wavelengths. Local environmental changes (such as stress or temperature changes) in OFI-based sensors can influence the length of the effective route of light propagation, causing the spectrum to vary. Based on this scenario, we must utilise expert spectrometers to determine the unknowns, such as bandwidth, wavelength, phase, intensity, and so on. Different optical devices, such as separators and mergers, are required in the simultaneous use of composite OFI to achieve the transmission of multiple beams in different fibers, introducing the phase difference between these beams. To streamline and miniaturize OFI setups, there have been proposals for in-line structures utilizing MMI along a single optical fiber. These structures offer a more compact alternative, enhancing the feasibility of integrating OFI technology into smaller-scale applications (Guo et al., 2007). In this dissertation, two OFIs: Microfiber Ring Resonator (MRR) and Singlemode-Multimode-Singlemode (SMS) optical are developed for sensing and laser applications. This section mainly describes the working principle, fabrication, and characteristics of both filters.

3.2 Microfiber Ring Resonator

Optical microfibers (MFs) obtained from ordinary single mode fibers (SMFs) are appealing because they are less expensive, easier to couple to SMFs, and have much lower loss than most lithographically manufactured waveguides (Chen et al., 2009). At 1550nm wavelength, the average propagation loss of a MF with micrometer-scaled width is less than 0.1dB/mm (Lim et al., 2012a) . Furthermore, MFs have enabled the development of micro-instruments such as fiber couplers, microfiber resonators and fiber sensors. The MRR stands out as a distinctive optical micro-resonator, fashioned from a fiber loop with a diameter spanning several microns. Comprising straight fiber sections bent into a closed

loop, MRR facilitates resonant behaviour as light traverses around the ring. This resonator can be coupled with the fiber via a conical fiber or waveguide. While currently applied prominently in optical communication systems, particularly for signal processing and pulse shaping applications due to its high nonlinear effect and all-fiber structure, MRRs exhibit substantial potential for development in sensing applications, particularly in substance detection. This dissertation introduces an innovative microfiber ring resonator (MRR) sensor designed specifically for detecting solution concentrations. The MRR sensor is made by meticulously stretching and bending a standard silica fiber (SMF-28) into a circular configuration, achieved through precise heating with high-temperature blue fire generated from pure oxygen and gas. In this section, the working principle, fabrication, and characterization of the MRR are described.

3.2.1 Working Principle of MRR

The basic working principle of MRR as a substance detection sensor relies on the wave principle of light, namely the resonance effect. The wavelength of the resonance wave in the output spectrum is adjusted by exploiting the strong evanescent field to perceive changes in surrounding media properties. In an idealized case, we assume that the loop is a regular circle. Under this premise, we can ignore the relationship between the field distribution in the loop and the specific axial position of the theoretical simulation, so that the transmission invariant number β and the coupling invariant number k are regarded as constant functions of the axial position (Shi et al., 2007). Therefore, the fundamental concept of ring resonators states that the transmission can be expressed as (M. Sumetsky et al., 2006) :

$$T = \frac{e^{(-\alpha L)} + \sin^2(k\Delta L) - 2e^{\left(-\frac{\alpha L}{2}\right)} \sin(k\Delta L)\cos(\beta L)}{1 + e^{(-\alpha L)} \sin^2(k\Delta L) - 2e^{\left(-\frac{\alpha L}{2}\right)} \sin(k\Delta L)\cos(\beta L)} \tag{3.1}$$

where, α is the intensity attenuation coefficient (i.e., the power attenuation coefficient of this model), L is the loop length, and ΔL is the coupling zone length. According to Eq. (1), when $\beta L = \frac{\pi}{2} + K\pi$, and K is an integer, resonance phenomenon occurs in the transmission spectrum.

Because of generating resonance spectrum, Q-factor of MRR, that is, the expression from resonance wavelength λ to the full half-peak width of the corresponding resonance spectrum, can be written as (M. Sumetsky et al., 2006):

$$Q = \frac{\lambda L}{k^2(\Delta L - \Delta L_m)^2 + \alpha L} \cdot \frac{\partial \beta}{\partial \lambda} \tag{3.2}$$

where, $\Delta L_m = \frac{\frac{\pi}{2} + K\pi}{k\beta}$, K is an integer, and $\alpha L \ll 1$.

The basic principle of this experiment is to change the effective RI n_{eff} of the guide mode in the microfiber ring by changing the RI n_a of the medium in the environment of the MRR, thus causing the displacement of the resonant wavelength λ_r. According to the sensing principle, its sensitivity can be expressed as (Chung-Yen & Guo, 2006):

$$S = \frac{\partial \lambda_r}{\partial n_a} = \frac{\partial \lambda_r}{\partial n_{eff}} \cdot \frac{\partial n_{eff}}{\partial n_a} \tag{3.3}$$

3.2.2 Construction and Characterization of MRR

The primary optical component in this study is the MRR, created through the formation of a ring structure using a microfiber. The microfiber is carefully fabricated from a standard SMF employing a flame-heated taper-drawing technique. To initiate the experiment, a segment of the optical fiber is stripped of its external coating and securely affixed to a custom fiber tapering machine (refer to Fig. 3.1 (a)). The stripped standard SMF is held in place by two fiber holders attached to independent translation stages, one of which is stationary and the other is a motorised stage capable of one-dimensional movement at a controlled speed.

The process of fabricating the tapered fiber involves heating it to its softening temperature and subsequently pulling the ends apart to reduce the radius of the fiber to approximately 0.5-2μm (depicted in Fig. 3.1 (b)). Accomplished using a high-temperature and stable micro-burner fuelled by clean butane gas mixed with pure oxygen, the tapering process demands precision. The micro-burner, mounted on a movable stand, is capable of vertical swinging to flame-brush the tapered fiber. Maintaining a clean flame and meticulous control of the burning gas flow are essential to prevent air convection from compromising the integrity of the fiber during the drawing process. To guarantee uniform heat distribution, the flame is applied to the fiber at an optimised angle.

The MRR is created by intricately coiling the microfiber upon itself through the interplay of two surface forces: the Van der Waals force and electrostatic force. These forces serve to counteract the elastic force, maintaining the stability of the loop by preventing the fiber from straightening. Once fabricated, the MRR is carefully positioned on a pre-prepared glass slide. By methodically controlling the slow outward pulling of both ends of the microfiber, a well-defined ring structure is meticulously formed. Refer

to Figs. 3.1 (c) and (d) for a visual representation of the fabricated MRR structure, showcasing loop diameters of approximately 285.6 µm and 379.3 µm, respectively. Recognizing the challenge of relying solely on Van der Waals and electrostatic forces to sustain the geometric parameters in the overlapping area of microfibers, it becomes imperative to swiftly secure both ends of the microfiber after the ring structure is established. This rapid fixation ensures the structural stability of the micro-ring. Subsequently, the MRR is subjected to examination under an electron microscope to precisely determine its specific parameters.

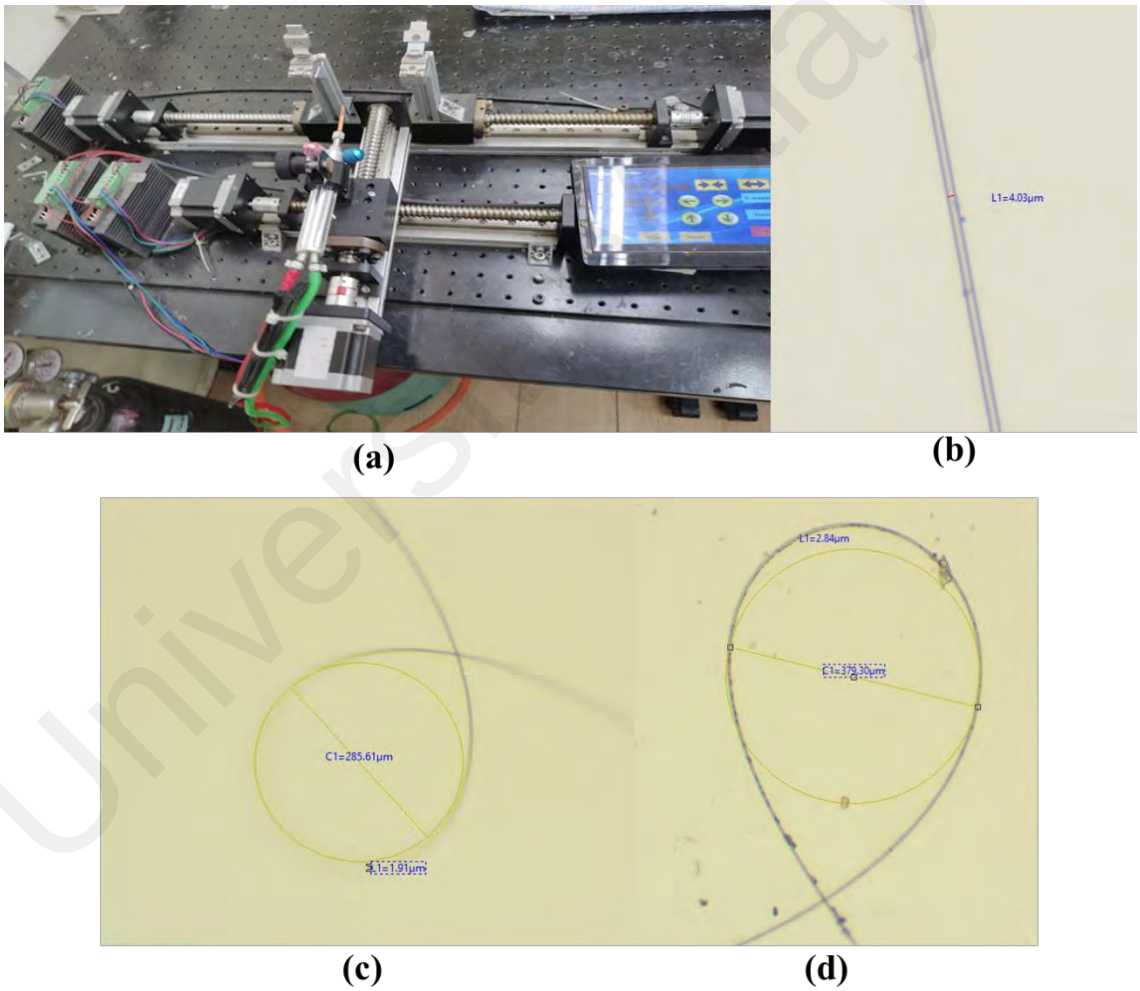

Figure 3.1: (a) Microfiber fabrication setup, (b) the fabricated microfiber, (c) MRR with a loop diameter of 285.6 µm, and (d) MRR with a loop diameter of 379.3 µm

Based on the preceding section's theories, one end of the MRR was coupled to an ASE source at 1550nm, while the other end was coupled to OSA to measure the propagation spectrum. The experimental setup is shown in Fig. 3.2 (a). A MRR exhibits a comb propagation spectrum akin to a Fabry–Perot filter. The resonant wavelength adheres to the condition $\lambda_m = \frac{2\pi R n_{eff}}{m}$, where R signifies the ring's radius, n_{eff} is the effective RI of the ring, and m represents the resonant mode number. The FSR, denoting the resonant frequency spacing, is determined by (M Sumetsky et al., 2006):

$$FSR = \frac{c}{2\pi R_{eff}} \tag{3.4}$$

where c is the velocity of light in a vacuum. The Q-factor of a ring resonator finds expression as:

$$Q = \frac{\lambda_m}{\Delta\lambda_{FWHM}} \tag{3.5}$$

where $\Delta\lambda_{FWHM}$ stands for the ~3dB bandwidth of the centre peak. A higher Q is achieved with a lower coupling coefficient between the ring and the straight waveguide. The proper selection of the ring's radius and connection coefficient aids in achieving the optimum resonant frequency spacing and resonant peak bandwidth. The connection coefficient is affected by the overlapping area, effective RI, and tapered fibre diameter.

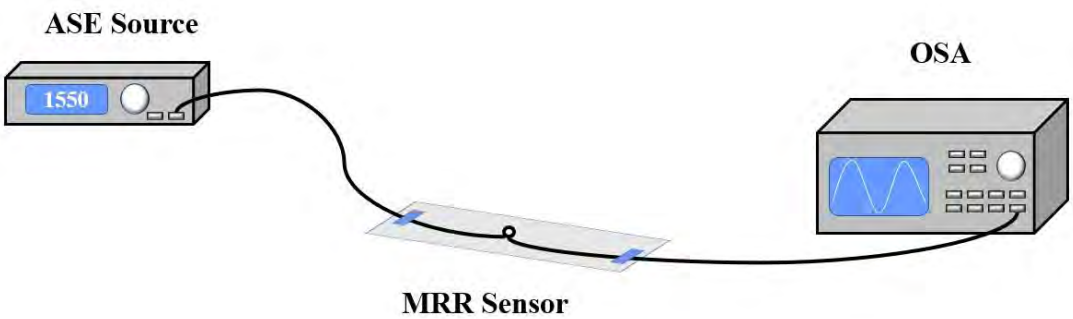

(a)

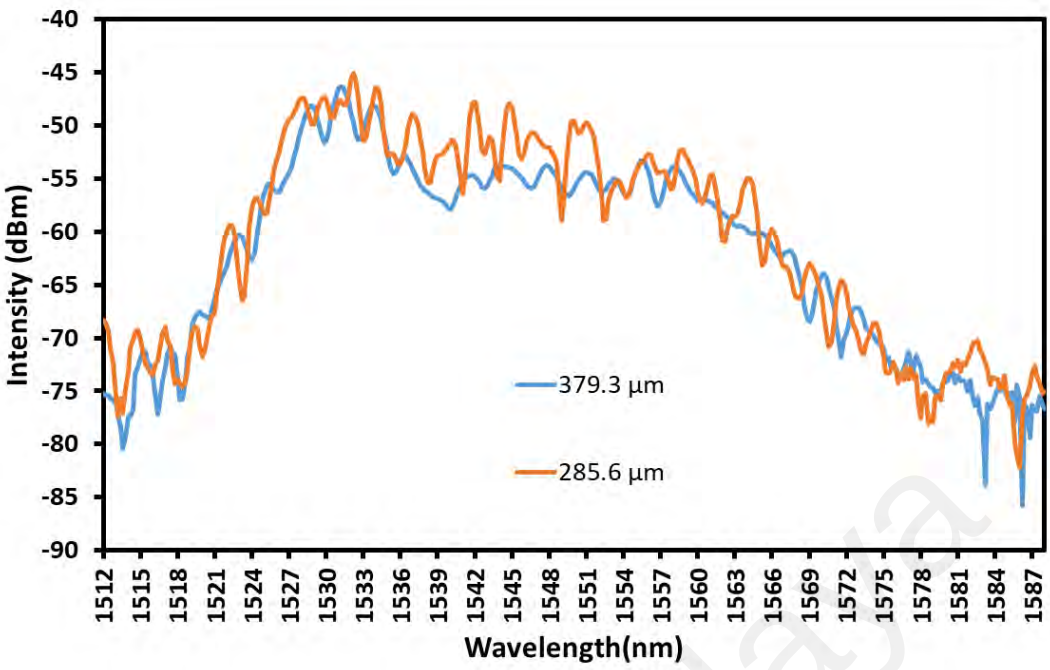

(b)

Figure 3.2: (a) microfiber characterization setup, and (b) the measured transmission spectrum for two different MRR samples

The measured comb propagation spectra of the MRR are shown in Fig. 3.2 (b), which were obtained by using the ASE source in conjunction with OSA for two different samples with the loop diameters of approximately 285.6µm and 379.3µm. The resonant response of the MRR is obvious. The smaller loop diameter indicates a better extinction ratio.

3.3 Singlemode-Multimode-Singlemode (SMS) Structure

Multiple beams are often transmitted along independent optical fibers or various routes within a single optical fiber in an optical fiber interferometer. When these independent beams are merged, they interact and interfere. This interference can have either positive or negative consequences, exhibiting as the transmission of light fluctuates over a wide range of frequencies. Small changes in the external environment, such as mechanical

force or temperature fluctuations, will modify the effective propagation path length of light in the optical fiber, resulting in the waveform displacement phenomena. Based on this scenario, we must utilise expert spectrometers to determine the unknowns, such as bandwidth, wavelength, phase, intensity, and so on (Lee et al., 2012). In the simultaneous usage of the standard fiber interferometers, several optical devices, such as separators and mergers, are necessary to achieve the transmission of multiple beams in distinct fibres, introducing the phase difference between these beams. In-line structures utilising MMI along only one fiber have been suggested to streamline and miniaturise optical fiber interferometers (L. B. Soldano & E. C. Pennings, 1995). These structures, more compact in nature, fall into three primary categories of the MMI: Fabry-Perot Interferometer (FPI) (Zhang et al., 2020), Sagnac Loop Interferometer (Reyes-Vera et al., 2017), and Singlemode-Multimode-Singlemode (SMS) fiber structures (Wang et al., 2008b).

An FPI is a component consisting of two surfaces that never touch each other, separated by a fixed distance. Light waves accrue a wavelength-dependent phase difference as they travel across these surfaces, resulting in interference at convergence. Fiber-based FPIs are classified as intrinsic or extrinsic based on the position of the reflectors in relation to the fibers. The reflecting components of an intrinsic FPI are located within the fiber, as evidenced by structures such as micro-holes (Cao et al., 2020). An extrinsic FPI, on the other hand, places the reflecting components outside of the fibers, such as when an air gap is placed between two fiber ends (Rao, 2006).

The Sagnac loop is built by separating the light incident into the loop with fibre couplers and propagating the two beams in diametrically opposing directions. Furthermore, a fiber with a greater dual RI is inserted into the loop, and the phase of the light may be altered by adjusting the phase of its fast and slow axes to generate a stable

Sagnac loop interference light. The SMS fiber structure is a tiny length of MMF neatly spliced between two SMFS, as opposed to the fiber heterostructure, which is made up of several distinct types of fibers fused together. This structure's fiber has major advantages, including low cost, ease of manufacturing, high sensitivity, and structural stability, all of which are crucial properties in practical production applications. This section describes in depth the working concept, structure, and properties of the SMS structure.

3.3.1 Working Principle of SMS Structure

The SMSF structure is composed of a concise segment of the MMF that is fusion spliced between two SMFs. The operational principle of an SMSF structure hinges on MMI and the associated phenomenon of self-focusing. While SMSF finds application in various optical fiber systems, their predominant use lies in serving as sensors for a diverse array of parameters. These parameters span the macro-world, encompassing measurements of mechanical forces, environmental variables, and RI (Ridho et al., 2020). Furthermore, SMS structures extend their utility into the micro-world, enabling precise measurements of entities such as RNA, enzymes and organic compounds (Vollmer & Yang, 2012). This versatility positions SMS fiber structures as valuable tools in the realm of optical sensing across a broad spectrum of applications.

The SMSF structure is created by fusing a short section of the SIMF linking two SMFs, as illustrated in Fig. 3.3. As light travels through a SMF, it excites multiple modes, leading to periodic self-imaging along the MMF, where no phase difference exists between the excited modes. The light field distribution $E_{MM}(r, \phi, z)$ along the MMF can be expressed as:

$$E_{MM}(r,\phi,z) = \sum_{n=1}^{N} C_n e_n(r,\phi,z) e^{-i\beta_n z} = e^{-i\beta_1 z} \sum_{n=1}^{N} C_n e_n(r,\phi,0) e^{-i(\beta_n - \beta_1)z} \quad (3.6)$$

where C_n is the mode expansión coefficient, $e_n(r,\phi,0)$ is the n-th guided-mode of MMF, β_1 and β_n are the transmission constants of essential mode and the nth excited mode in the MMF, correspondingly. Self-imaging happens when all the modes satisfy the following condition:

$$(\beta_{n-}\beta_1)z = m_n 2\pi \ (m_n \ is \ integer) \quad (3.7)$$

Equation (3.7) can be rewritten with the effective RI of the optical fiber $\Delta n_{eff,n}$ and the length of the MMF segment L as:

$$\Delta n_{eff,n} L = m_n \lambda_0 \ (m_n \ is \ integer) \quad (3.8)$$

where λ_0 is the centre wavelength and

$$\Delta n_{eff,n} = \frac{(\beta_n - \beta_1)\lambda_0}{2\pi} \quad (3.9)$$

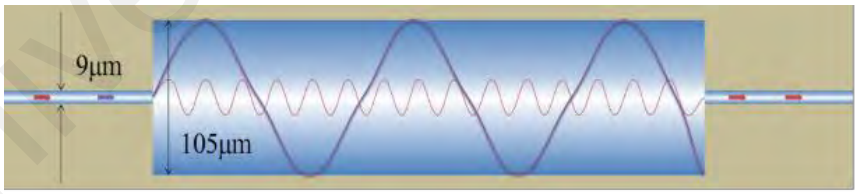

Figure 3.3: The schematic diagram of SMS structure

Equation (3.8) illustrates that the optical response of SMS structure relies on the effective RI, the length of the MMF, and the central wavelength of the light. To minimize the MMF length requirement, one can apply bending or stress to the fiber, inducing birefringence. This, in turn, results in additional nonlinear phase shifts as light traverses

through. The extent of the phase shift is contingent upon the level of birefringence, a factor manipulated by modifying the surrounding refractive index.

SMS structure is generally affected by MMI. When light enters the MMF in the form of a fundamental mode from the SMF end, some higher-order modes in the MMF will be positive and transmitted along their respective transmission constants and resulting wavelengths. Since different optical waveguide models have different propagation constants, resulting in different wavelengths, there is a phase difference in MMF propagation at the same time. Finally, these different modes of light will couple and become the fundamental mode again and enter the SMF at the other end. Then the output power can be expressed as (Tripathi et al., 2009):

$$P_{SMS} = \left| b_1^2 + b_2^2 e^{i(\beta_1 - \beta_2)L} + b_3^2 e^{i(\beta_1 - \beta_3)L} + \cdots \right|^2 \tag{3.10}$$

where β_i is the transmission constant of the i-th mode in the multi-mode, and b_i is the field amplitude, which is determined by the overlapping resonance of the essential mode of the SMF and the related modes in the MMF. From equation (3.10) it is clear that the power of the fiber varies with the length of the MMF section.

3.3.2 Construction and Characterization of SMS Structure

In this work, a 50mm long MMF was directly spliced with a standard SMF on each side to form the SMSF structure. The core diameter of the MMF is 105µm and the cladding is 125µm. Fig.3.4 (a) depicts the SMSF structure conceptually. The transmission spectrum is then measured by connecting one end of the SMS structure to an ASE source centred at wavelength of 1550nm while the other end was connected to OSA as shown in

Fig. 3.4 (b). Fig. 3.4 (c) depicts the SMS structure's spectrum propagation characteristic. It displays a periodic interference pattern caused by MMI caused by many stimulated modes as the laser light travels through the MMF.

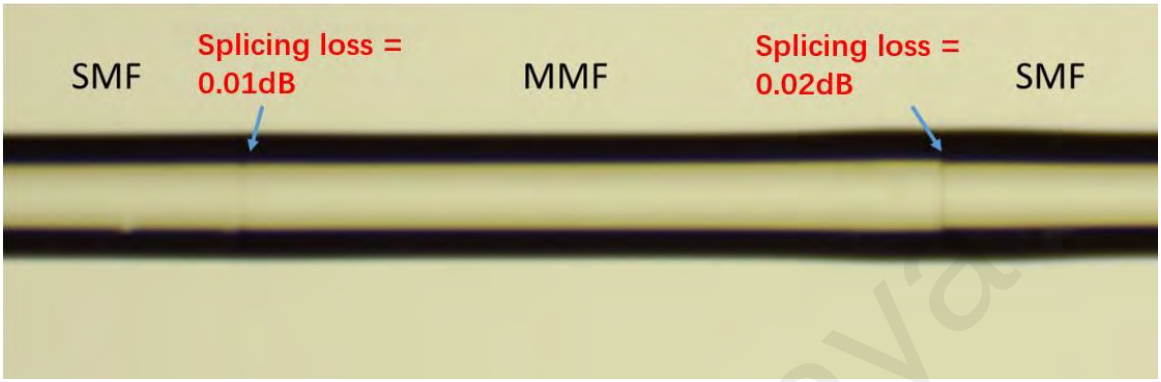

(a)

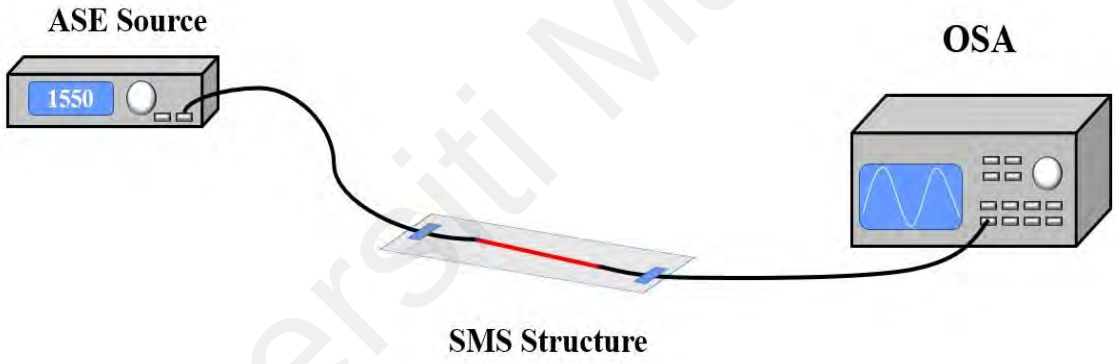

(b)

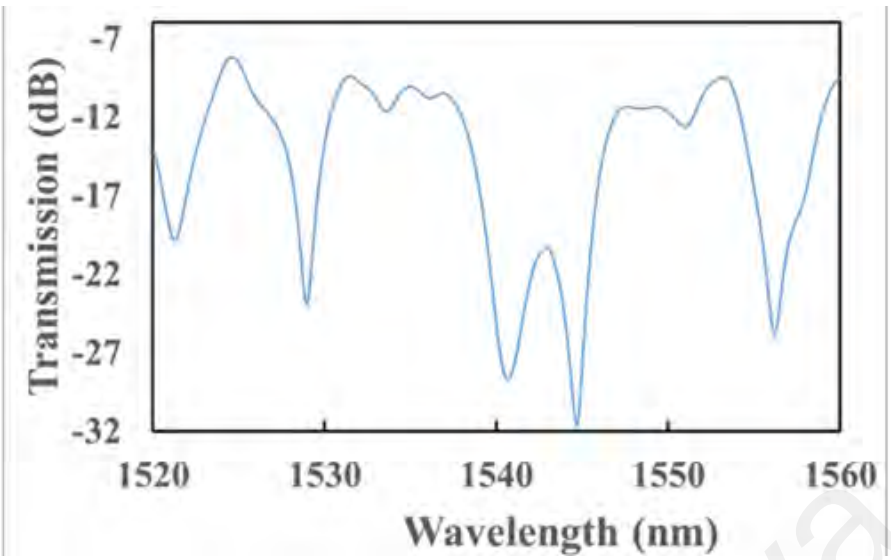

(c)

Figure 3.4: (a) Loss of SMSF structure after splicing, and (b) SMSF characterization setup, and(c) the spectral propagation characteristic of the SMSF structure

CHAPTER 4: SENSOR APPLICATIONS

4.1 Introduction

Optical sensors offer a promising alternative to conventional electronic sensors, thanks to their distinctive advantages, including swift response times, immunity to electromagnetic interference, and the absence of electrical signals (Lukose et al., 2021). These attributes hold significant value in various fields, notably in biomedical applications such as thermotherapy (Aslam et al., 2023) and the development of magnetic resonance-compatible sensors (Presti et al., 2020). Additionally, their utility extends to harsh environmental sensing. Researchers have also identified common optical materials where, based on their conduction characteristics and the interplay between light and matter, optical signal results can be effectively analyzed (Ma et al., 2021). This analysis aids in determining the material composition and other key properties of the test sample.

Currently, fiber-based sensing technologies have garnered significant interest due to their notable advantages, such as high sensitivity, compact size, and seamless integration (Xu et al., 2014). This chapter discusses the application of the prepared microfiber ring resonator (MRR) and singlemode-multimode-singlemode fiber (SMSF) structure for temperature and glycerin concentration sensing.

4.2 MRR for Temperature Sensing Application

Many applications for optical MF-based temperature detectors have been proposed, including medicinal, geological, automotive, and defence applications. The large measuring range, high sensitivity, and quick reaction of these highly integrated measuring equipment may explain their extensive use. Furthermore, in severe circumstances, these gauges can be performed remotely for field measurements. This section demonstrates

MRR based temperature sensing. Optical interferometers are one of the most commonly used optical measurement tools because they translate a change in the wavelength length or RI of a light wave into a shift in the phase of the light wave and a change in the intensity of the light intensity, and can thus be measured with extraordinary precision. The MRR is of interest as a miniaturised optical interferometer for phase-sensitive optical measurements with a small size and great sensitivity. In the experiment, the temperature control instrument was used to stably change the ambient temperature of MRR and record the output spectral results for analysis.

Figure 4.1 shows the output spectrum of MRR with waveform changes recorded every 5°C. From this image, it can be clearly observed that between the wavelength of 1536-1540nm, the output image of MRR at different temperatures has a relatively obvious displacement phenomenon. It can be more clearly shown in Figure 4.1 that the wavelength displacement of MRR output waveform is basically maintained at 0.2 nm for every 5°C increases between 55-75°C (excluding the error value caused by system error and measurement error). Based on the data in Figure 4.1, the wave-temperature linear image and intensity temperature linear image can be obtained by extracting the trough points of each temperature for data analysis, which are shown in Figure 4.2 and Figure 4.3 correspondingly. From the data analysis results, the change of ambient temperature within a certain range is positively correlated with the wavelength of MRR output spectrum. When the ambient temperature is between 55℃ and 75℃, the sensitivity of MRR is 0.18nm/℃ and the linearity is 0.8804 (Li et al., 2020). Fig. 4.3 shows the transmitted light intensity at different temperature points when the MRR structure becomes unstable due to the gradual increase in temperature. When the ambient temperature changes from 55°C to 75°C, the transmitted light intensity of the MRR changes between -41.3 and -47.4 dBm, with a rate of 0.1587 dB/°C and a linearity of less than 10%. The increase in temperature

will reduce the stability of the overall MRR structure and affect the transmission characteristics of the entire sensing structure.

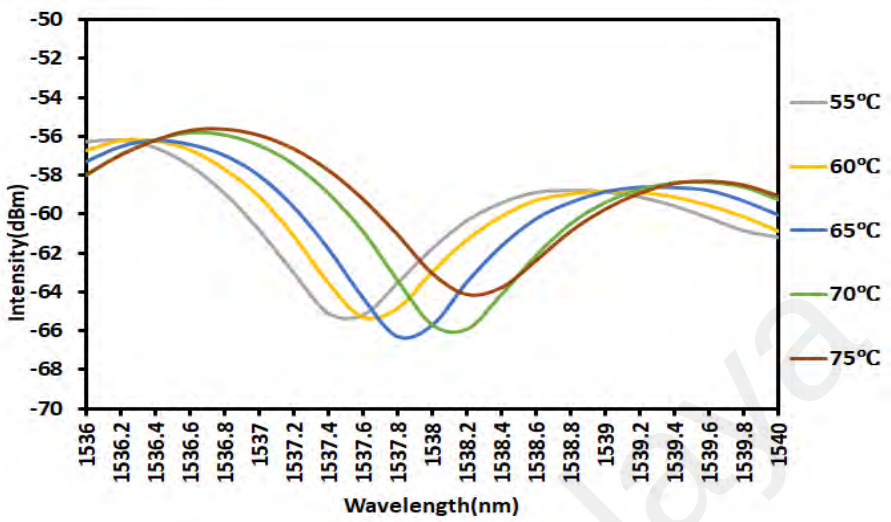

Figure 4.1: Output spectra of MRR at different temperature

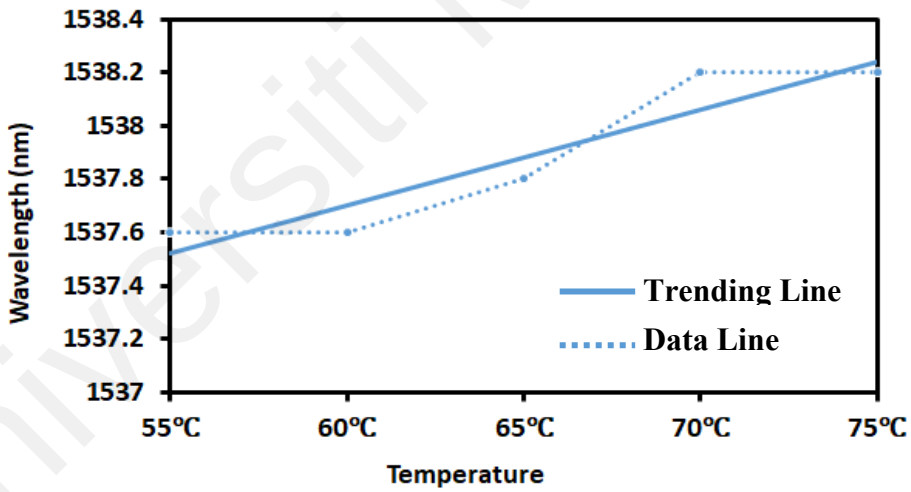

Figure 4.2: The wavelength shifting against temperature

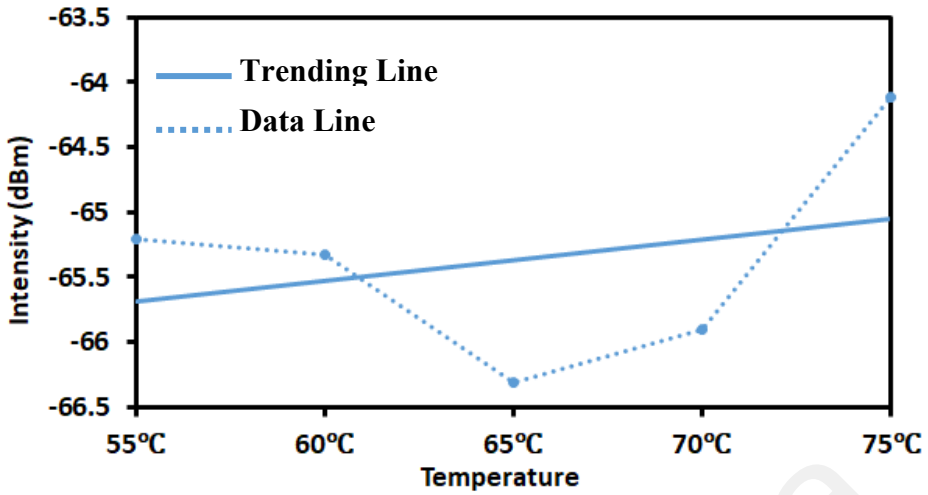

Figure 4.3: The transmitted light intensity from the MRR sensor with varying temperature

4.3 MRR for Liquid Refractive Index Sensing

The optical sensing technique stands out as one of the most widely employed approaches for substance detection. By examining the interaction of a sample with the wave characteristics of light, analysts scrutinize absorption, scattering, and transmission spectra to determine the properties of material composition (Kumar & Singh, 2021). This method not only claims simplicity in operation but also achieves high accuracy. Moreover, its non-contact nature, rapid detection capabilities, and heightened sensitivity make optical sensors a preferred choice over conventional electrical sensors. Currently, fiber-based sensing technologies are garnering considerable attention due to their inherent advantages, including high sensitivity, compact size, and seamless integration possibilities (Zain et al., 2020).

In contemporary research, there is a burgeoning fascination with refractive index (RI) sensors, particularly in the realm of label-free optical biosensing (Lukose et al., 2021). Binding events, ranging from DNA hybridization and antibody-antigen recognition to

chemical reactions and alterations in concentration, typically induce modifications in the surrounding environment of the optical sensor, consequently influencing the RI (Asghari et al., 2021). This alteration in RI serves as a quantitative indicator of the biosensor's detection prowess. Hence, the precise measurement of minute changes in RI resulting from biochemical processes emerges as a crucial element in the effective detection of biomarkers.

Fiber optic-based RI sensors are preferred for their label-free nature and versatile configurations. Among the most prevalent designs are Bragg grating structures (Sahota et al., 2020b), Mach–Zehnder interferometers (Li et al., 2021), tapered optical fibers (Syuhada et al., 2021), and micro-resonators (Zain et al., 2020). Notably, the microfiber ring resonator (MRR) stands out as a distinctive optical micro-resonator, fashioned from a fiber loop with a diameter spanning several microns. Comprising straight fiber sections bent into a closed loop, MRR facilitates resonant behaviour as light traverses around the ring. This resonator can be coupled with the fiber via a conical fiber or waveguide. While currently applied prominently in optical communication systems, particularly for signal processing and pulse shaping applications due to its high nonlinear effect and all-fiber structure, MRRs exhibit substantial potential for development in sensing applications, particularly in substance detection (Gai et al., 2017).

This section presents a new MRR sensor for sensing the concentration of solution. The MRR sensor is produced by stretching and bending a standard silicon fiber (SMF-28) into a ring using high temperature blue fire heating made of pure oxygen and gas (Zhang et al., 2011). The study explores into the sensor's performance by systematically observing variations in MRR transmittance across different concentrations of the same solution. The findings shed light on the sensor's efficacy and establish its potential as a reliable tool for solution detection, offering valuable insights for practical applications.

4.3.1 Experimental Arrangement

The main optical element in this study is MRR, which is made of MF. The MF is manufactured from a standard SMF using flame-heated taper-drawing technique as described in the previous chapter. In this experiment, standard SMF is also used as raw material. One section of optical fiber is stripped of its external coating and fixed on a homemade fiber tapering machine. Furthermore, high-temperature blue flame made from butane gas mixed with pure oxygen is employed to heat the stripped glass fiber so that it can be stretched to reduce the fiber diameter to around 1.9µm. The obtained microfiber was placed on a slide and bent to form a large ring structure. By controlling the slow outward pulling of both ends of the microfiber, a ring structure with a diameter of approximately 285.6µm was formed as shown in Fig. 4.4 (a).

The experimental setup is shown in Fig. 4.4 (b), in which one end of the MRR was connected to an ASE source centred at wavelength of 1550nm, and the other end was connected to OSA to measure the transmission spectrum. To verify whether MRR can be used as a liquid sensor, the ultimate purpose of this experiment is whether it can distinguish different concentrations of glycerin/water. During this experiment, the output spectrum of the MRR was recorded at different concentrations of glycerin (propane-1,2,3-triol) in water.

.

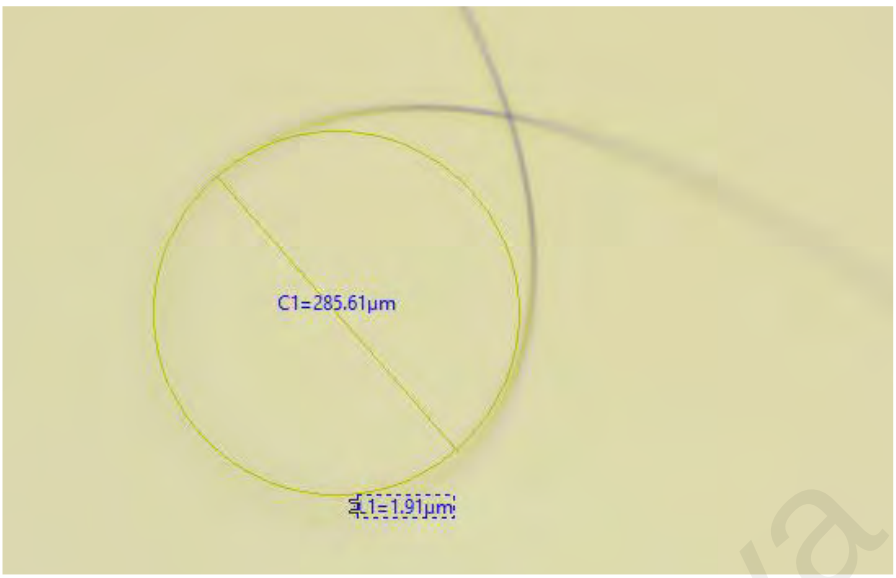

(a)

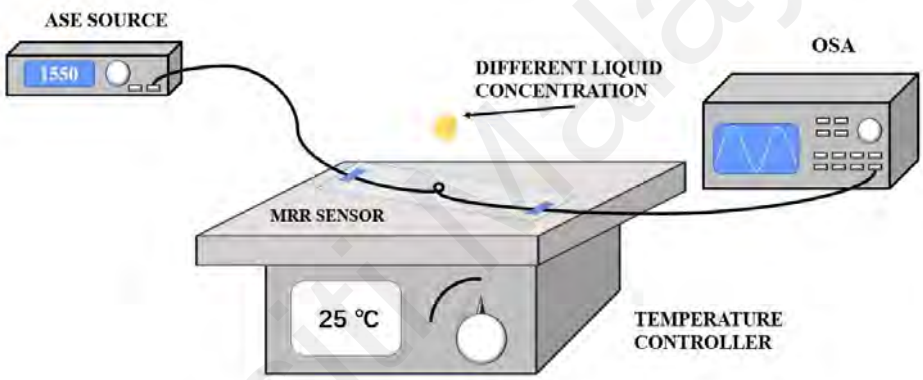

(b)

Figure 4.4: (a) microscope image of MRR structure, and (b) Experimental setup of the MRR based liquid sensor

4.3.2 Sensor Performance

Under the condition of keeping the ambient temperature stable at 25℃, we placed MRR in glycerin aqueous solution with 20% to 60% concentration respectively, and recorded the waveform change with each 10% concentration, as shown in Fig. 4.5. It is observed that the MRR output image has a relatively obvious displacement phenomenon between the wavelength of 1527-1536 nm. The wave crest points of each concentration in the band were extracted as characteristic values for fitting analysis, and the linear image

of wavelength and concentration was obtained, as shown in Fig. 4.6. The change of glycerin water concentration in a certain range is positively correlated with the wavelength of MRR output spectrum. When the solution concentration is between 20% and 60%, the sensitivity of MRR is 0.22nm/%Vol, and its linearity is 0.9528. This finding proves the feasibility of MRR as glycerin solution sensor.

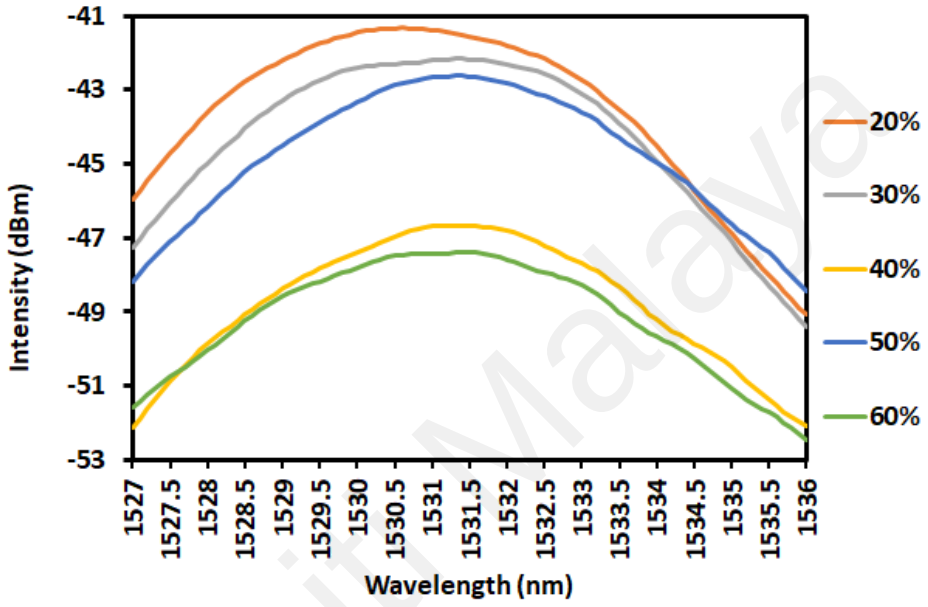

Figure 4.5: Output spectra of MRR at different glycerin liquid concentrations

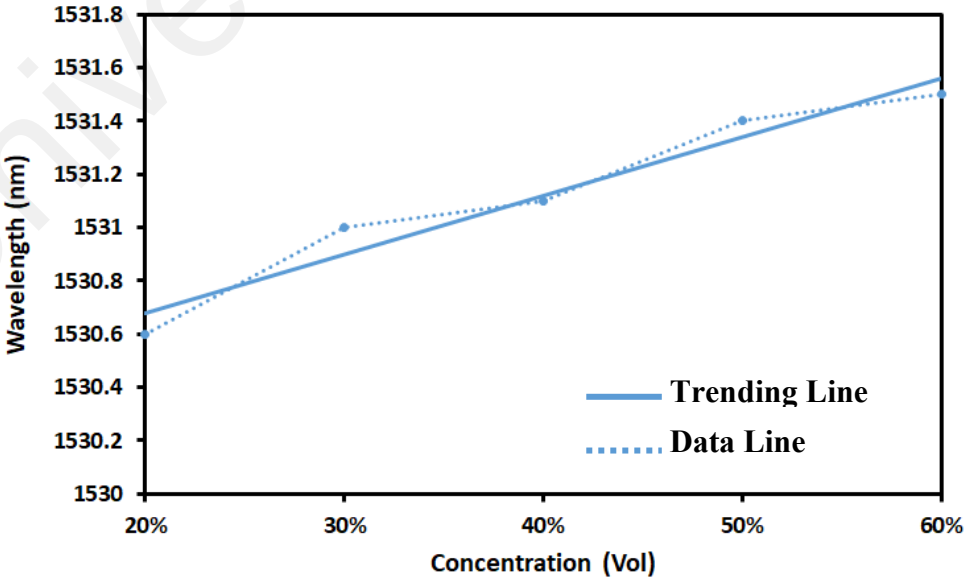

Figure 4.6: The wavelength shifts against the liquid concentration

Fig. 4.7 shows the intensity of the propagation light of the MRR when the structure was dropped by different glycerin liquid concentrations in water. The transmitted light intensity from the MRR varies from -41.3 to -47.4 dBm with a rate of -1.25 dB/%Vol and linearity of more than 50% as the liquid concentration is changed from 20 to 60%. As concentration enhances, the RI of the cladding changes, altering the propagation characteristics of the entire sensing system. The intensity of the output light decreases as the cladding RI increases. This is due to the increase in RI, which reduces the contrast in RI between the cladding and the core, allowing more light to escape and increasing losses.

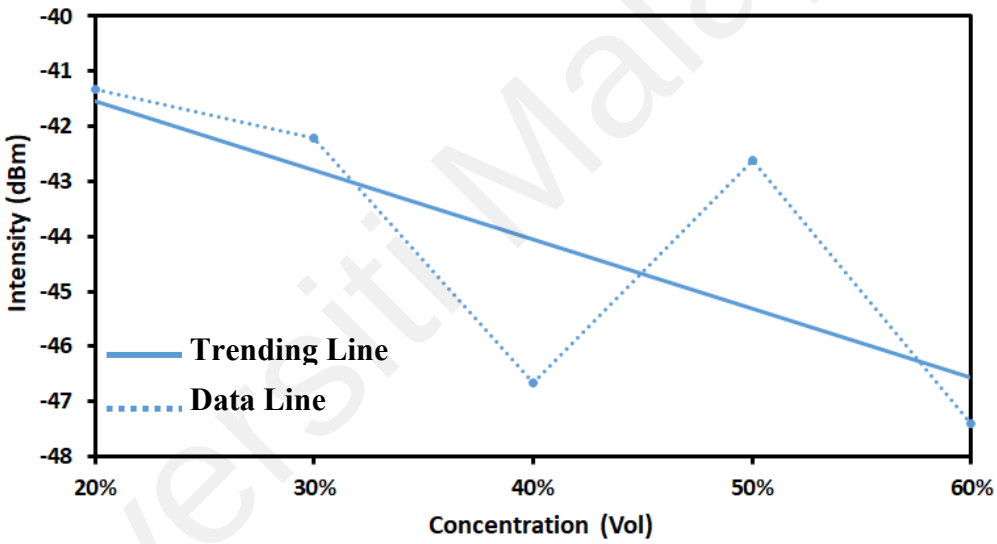

Figure 4.7: The propagated light intensity from the MRR sensor with varying liquid concentrations

4.4 SMS Structure for Temperature Sensing Application

In this section, a new approach for temperature sensing is demonstrated using an SMS structure as a sensor probe. While ensuring that other external environments did not change, the prepared SMS sensor was placed on the hot plate with a temperature controller and the waveform changes every 5°C from 55°C to 75°C were recorded, as

shown in Fig. 4.8. Through recording and observation, it was found that the MRR output spectrum image has a relatively obvious shift phenomenon between the wavelengths of 1552nm and 1562nm. The trough points at each temperature point in the band are extracted as feature values for fitting analysis, and a linear image of wavelength and temperature is obtained, as shown in Fig. 4.9. Changes in ambient temperature within a certain range are negatively correlated with the wavelength of the SMS output spectrum. When the ambient temperature is between 55℃ and 75℃, the sensitivity of the SMS sensor is -0.80nm/℃ and the linearity is 0.9854.

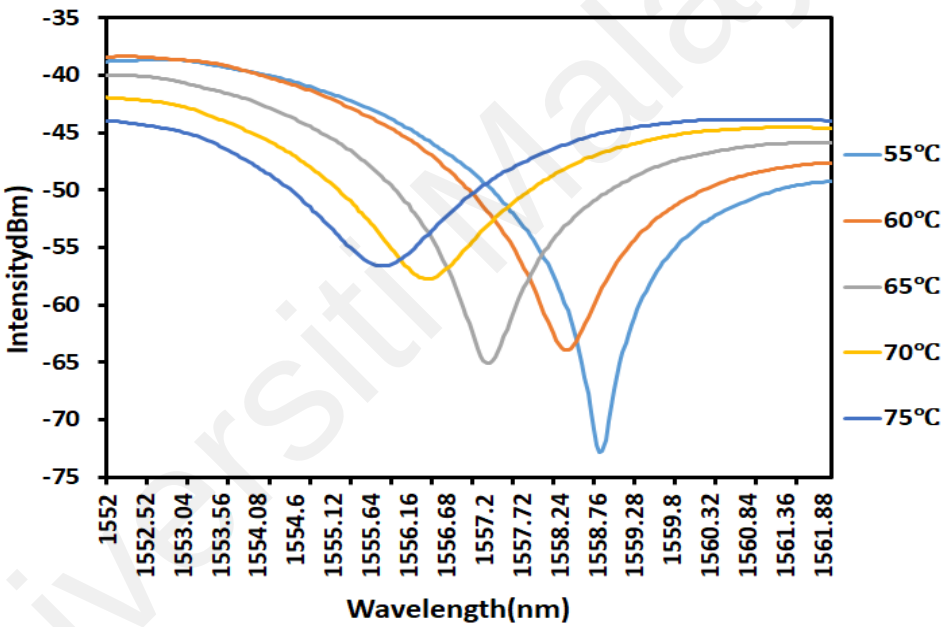

Figure 4.8: Output spectra of the SMS sensor at different temperature

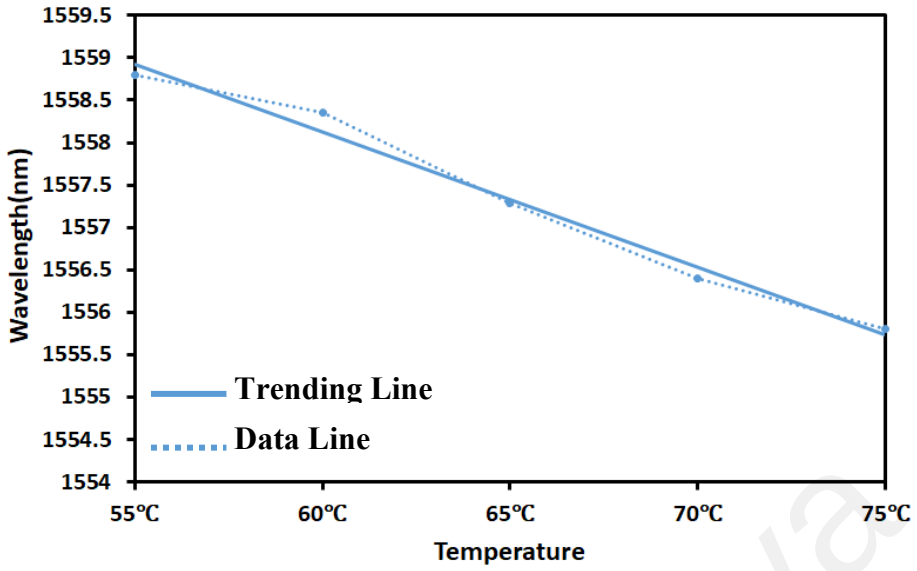

Figure 4.9: The wavelength shifts against temperature

Fig. 4.10 shows the transmitted light intensity at different temperature points as the higher-order modes of SMS structure are continuously positive due to the gradual increase in temperature. When the ambient temperature changes from 55°C to 75°C, the transmitted light intensity changes between -73 and -56 dBm, with a rate of 3.8605dB/°C and a linearity of 0.8753. The increase in temperature will excite the high-order modes in MMF to a certain extent, thereby increasing the degree of coupling with the enesstial mode of SMF, affecting the propagation features of the entire sensing structure.

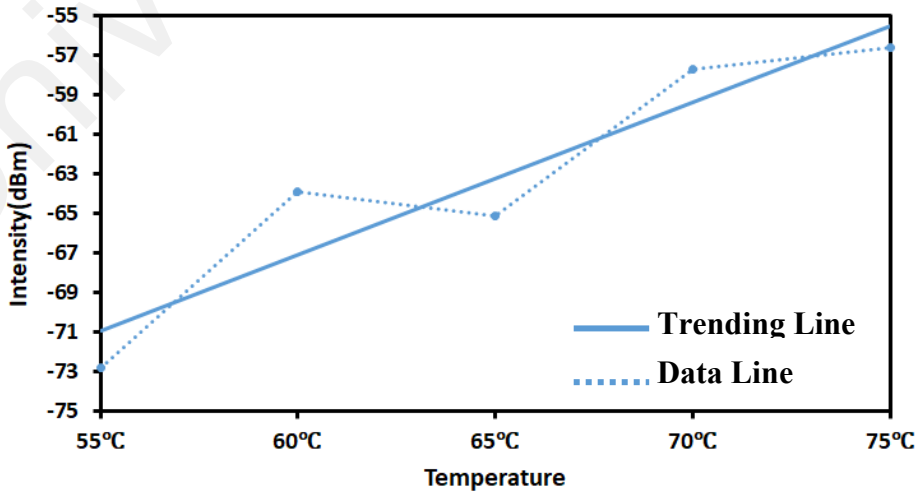

Figure 4.10: The propagated light intensity from the SMS sensor with varying temperature

4.5 SMS Structure for Liquid Refractive Index Sensing

In this section, a new approach to glycerin concentration sensing is demonstrated using a modified SMS sensor. Unlike conventional SMSF structures that utilize a short section of standard MMF, this study introduces a novel approach by replacing the MMF with a tapered fiber. The modified SMS structure is specifically showcased for its efficacy in temperature and liquid refractive index sensing. Notably, the substantial sensing responses to temperature change and varying concentrations of glycerin (propane-1,2,3-triol) in water are observed, attributable to the shifts in cladding refractive index. Given the extensive utilization of glycerin across diverse industries and the imperative for stringent quality control, regulatory compliance, and process optimization, testing glycerin solutions holds significant importance (Pharmacopoeia, 2014).

4.5.1 Experimental Arrangement

For liquid sensing application, the cladding of the MMF should be removed. At first, the fiber is spliced to a SMF in both ends to form a SMS structure. After completing the production of the SMS optical fiber structure, connect one end to the ASE source and the other end to the OPM. Straighten the multimode optical fiber and place it on a polishing wheel with sandpaper attached and fix it with fiber holders. During the production process, the PD of the multimode fiber was determined by observing the numerical changes of OPM. In this experiment, the PL was ensured to be less than 3dB during the production process. The SMS structure and fiber types used in (Tang et al., 2017) are the same as those in this experiment. When 5μm<PD<70μm, PL will increase with the increase of PD and has an obvious linear relationship. The formula is as follows:

$$PL = 0.048 \times PD - 0.15499 \tag{4.1}$$

It can be seen that the PD is 65.73μm , and the total loss of the side-polished fiber

produced in this experiment is 10 dB. In addition, the structural change of MMF fiber through side-polished D-shaped destroys the original symmetry characteristics of MMI, which stimulates more high-order modes in MMF and allows more light to escape to enhance the evanescent field effect. Based on these theories, one end of the SMS structure was linked to an ASE source centred at wavelength of 1550nm, and the other end was linked to OSA to measure the transmission spectrum. The experimental setup was shown in Fig. 4.11. During this experiment, the output spectrum of the SMS was recorded at different temperatures and concentrations of glycerine (propane-1,2,3-triol) in water.

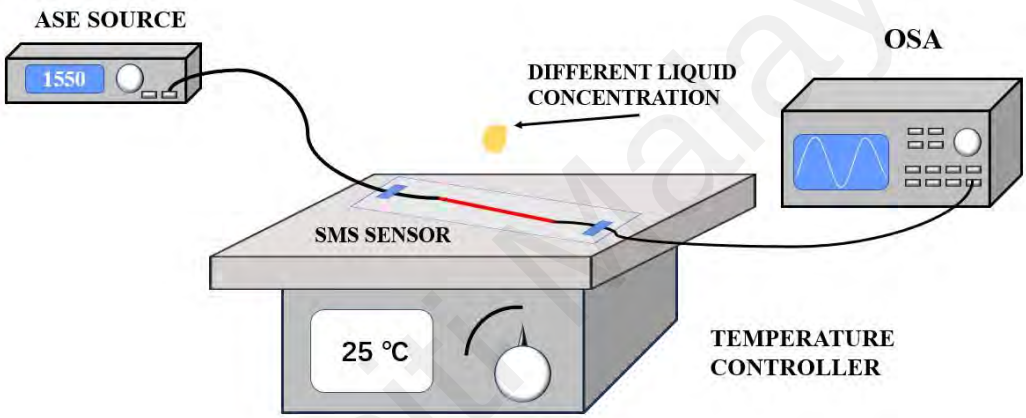

Figure 4.11: Experimental setup of the SMS based glycerin concentration sensor

4.5.2 Sensor Performance

Under the condition of keeping the ambient temperature stable at 25℃, we placed the modified SMS structure with tapered MMF in glycerin aqueous solution. The solution concentration varied from 20% to 60%, and the waveform change was recorded with each 10% concentration, as shown in Fig. 4.12. It is observed that the output image has a relatively obvious displacement phenomenon between the wavelength of 1553-1560 nm. The wave crest points of each concentration in the band were extracted as characteristic values for fitting analysis, and the linear plot of wavelength and concentration was obtained, as shown in Fig. 4.13. The change of glycerin water concentration in a certain

range is positively correlated with the wavelength of SMS output spectrum. When the solution concentration is between 20% and 60%, the sensitivity of the sensor is -1.152nm/%Vol, and its linearity is 0.9821.

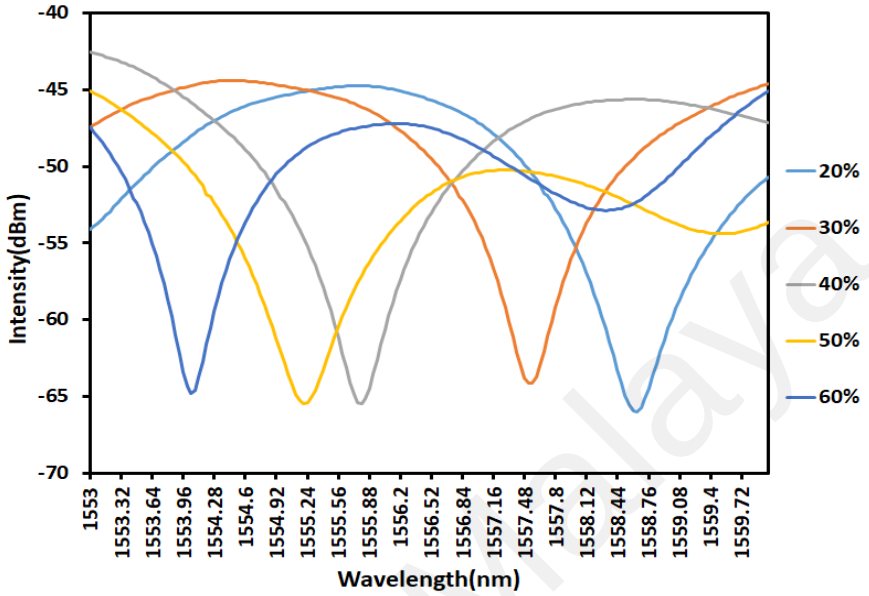

Figure 4.12: Output spectra of the modified SMS sensor at different glycerine liquid concentrations

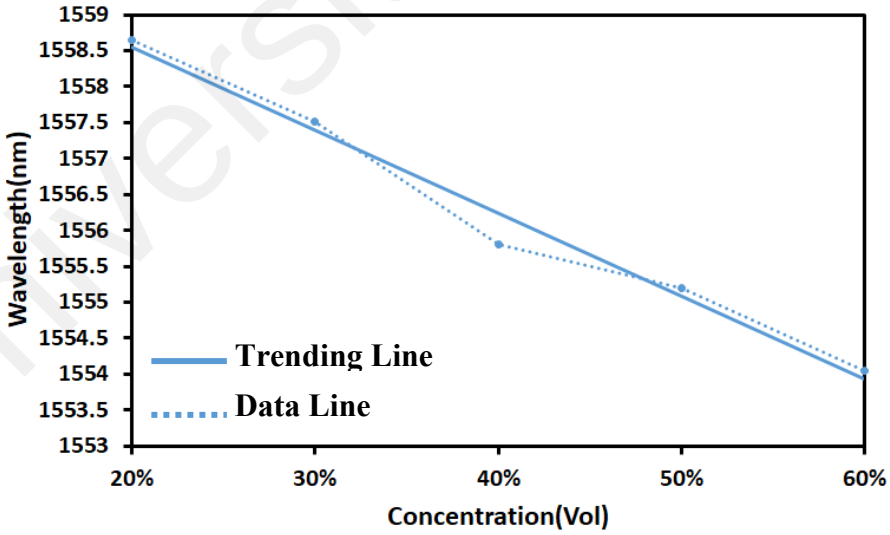

Figure 4.13: The wavelength shifts against the liquid concentration

CHAPTER 5: LASER APPLICATION

5.1 Introduction

When compared to other types of ultrafast lasers, mode-locked fibers lasers have garnered an enormous amount of emphasis in the past few years because of their benefits in the areas of dependability, cost effectiveness, high stability, and compactness (Xu et al., 2022). They have the ability to generate extremely brief, high-energy pulses with short pulse durations that range from femtoseconds to nanoseconds, which are required in many different kinds of applications including as material processing, telecommunications, nonlinear optics, and bio-photonics (Pierce et al., 2001; Shi et al., 2014; Shiner, 2016). Taking mode-locked lasers as an example, researchers' examination of it is of exceptional and necessary value for understanding nonlinear optical processes and building more cutting-edge photonics devices. These lasers are capable of producing parametric processes, harmonic harmonics, and ultrafast continuums for a variety of uses, including laser sources and imaging apparatus (Mary et al., 2014).

Saturable absorber (SA) is the key element in the mode locked fiber laser (Pang et al., 2022). It plays a pivotal role in initiating mode-locking operations within a fiber laser system, facilitating the synchronization of light wave phases within the laser cavity. Mode-locking success is dependent on attaining phase coherence among all optical modes, which results in constructive interference that amplifies the strength of transmitted pulses. The SA's natural capacity to switch from high absorption to high propagation is critical in attaining phase synchronisation, which eventually results in the generation of mode-locked pulses in the fiber laser cavity.

Up to date, many emerging new materials have been explored as SA to induce mode-locking in fiber laser systems. Examples include graphene (Haris et al., 2020), transition metal dichalcogenides (Li et al., 2022), MXene (Fu et al., 2021), topological insulators (Mondal et al., 2021), and certain organic materials (Samsamnun et al., 2020), all demonstrating their capacity to induce ultrafast phenomena in fiber laser systems. These materials share common qualities such as fast recovery times, robust nonlinear absorption, and broad spectral compatibility. Despite their promising attributes, these emerging materials face shared challenges, hindering their commercial viability. Issues like high manufacturing costs, thermal damage thresholds, and long-time stability constraints impede their widespread use. Consequently, the adoption of artificial SAs is emerging as a pragmatic alternative for inducing mode-locked fiber lasers.

The similar concept of SMF-MMF-SMF artificial SA had been reported before as shown in Table 5.1.

Table 5.1: Mode-Locked Fibre Lasers based on SMF-MMF-SMF Artificial SA.

SA Structure	Centre Wavelength (nm)	Pulse Width	Repetition Rate (MHz)	Mode-Locking Threshold (mW)	Ref.
SMF-GIMF-SMF with inter cavity	1558	528 fs	86.07	54	(Zeb et al., 2021)
Coiled SMF-GIMF-SMF	1564.71	559 fs	25	71	(Zhang et al., 2019)
SMF-GIMF-SMF	1571	675 fs	11.69	80.4	(Zhang et al., 2022)
SMF-GIMF-SMF	1584.8	510 fs	21.37	41.6	(Chen et al., 2024)

SMF-SIMF-SMF	1567	390 ns	1.28	189.2	This work

Artificial SAs are created by modifying optical substances to generate the SA effect. Multiple strategies to produce artificial SAs including nonlinear polarization rotation (NPR) (Gao et al., 2019), nonlinear optical loop mirror (NOLM) (J. Li et al., 2014), and nonlinear amplifying loop mirror (NALM) (Yu et al., 2018). These strategies have proven to be efficient in producing consistent and dependable mode-locking operations in fiber laser systems. Nevertheless, each approach has its specific requirements. To create light rotation, the NPR approach, for example, requires a long length of nonlinear material. The NOLM approach necessitates the use of a figure-of-eight cavity for the optical loop, but the NALM method necessitates the use of an extra amplifier to improve light oscillation within a figure-of-eight cavity. These requirements can contribute to the mode-locked fiber laser system becoming bulkier and may potentially lower the pulse repetition rate within the cavity. Addressing these challenges is crucial for optimizing the performance and practicality of artificial saturable absorbers in mode-locked fiber laser applications.

In this chapter, the application of the singlemode-multimode-singlemode fiber (SMSF) structure as an artificial SA to stimulate mode-locked is proposed and experimentally demonstrated. A SMSF structure is integrated into an Erbium-doped fiber laser (EDFL) system to stimulate mode-locked operation.

5.2 Laser Setup

The suggested mode-locked fiber laser, which uses an SMSF structure as a fictitious SA, is configured as seen in Fig. 5.1. One MMF is fusion spliced in between two standard SMFs. The length of the MMF is optimised to 50mm for maximum laser efficiency and mode-locked functioning at a lower threshold pump power. The auto fiber splicing mode of the FITEL 178A fusion splicer is used for splicing. The standard SMF used has core/cladding diameter of 9/125 μm, whereas the MMF has a core/cladding diameter of 105/125 μm. The MMF allows light to circulate as core and cladding modes. At a sufficient pump power, high intensity modes are capable of passing through the SMS structure with less loss, while low intensity modes are filtered by the artificial SA device. The transmission behavior of the SMSF structure is intricately linked to the self-imaging effect within the system. This phenomenon selectively permits the passage of high-power signals while attenuating low-power signals, effectively endowing the SMS structure with SA characteristics.

To initiate ion excitation in a 40 cm-long Erbium-doped fiber (EDF), a 980 nm pump laser is employed, facilitated by a wavelength division multiplexer (WDM). To maintain unidirectional circulation within the ring cavity, a polarization insensitive isolator is employed in the laser cavity. The integration of the SMS structure serves the purpose of an artificial SA, and an polarization controller (PC) that adjusts the waveform. An output coupler with a ratio of 50:50 completes the ring cavity, redirecting half of the circulating light back into the cavity, while the remaining half is extracted for further analysis. The additional 150 m long SMF is added into the laser cavity to increase the nonlinearity and balance the dispersion so that the mode-locking can be realized. The total length of the cavity is approximately 162 meters. Analyzing the mode-locked laser characteristics involves assessing the wavelength domain using an OSA (Anritsu MS9710C). In the time

domain, the pulse train is visualized using a photodetector (ET-3500F) and an oscilloscope (GW Instek GDS-3352). Lastly, the stability of the mode-locked operation is affirmed through a RFSA (MS2830A).

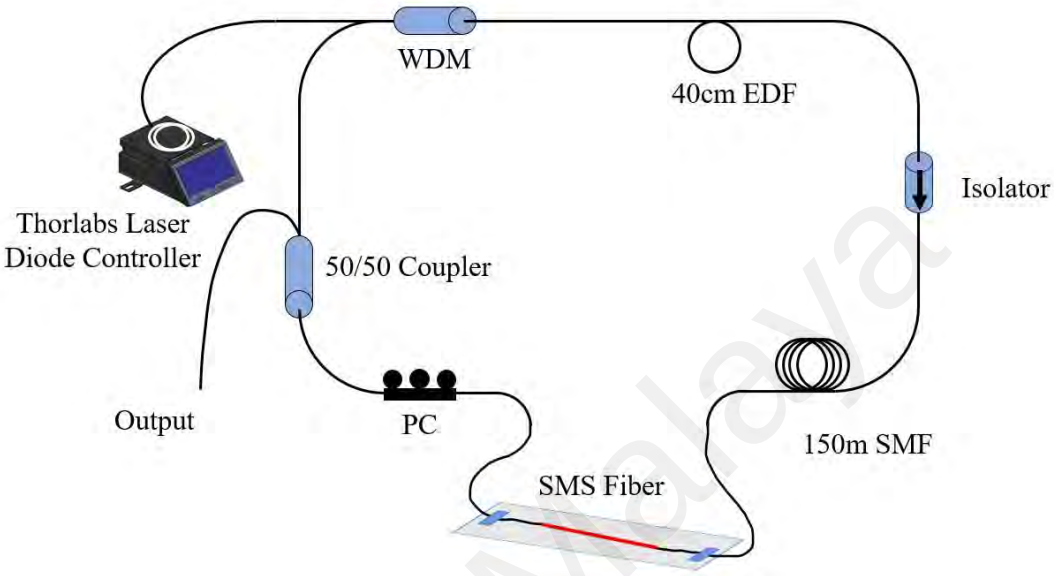

Figure 5.1: Experimental setup of indicated mode-locked EDFL with the SMSF structure, which functions as an artificial SA

5.3 Laser Performance

The SMS served as an artificial SA, phase-locking the longitudinal modes oscillating in the EDFL cavity and generating mode-locked operation. The MMF facilitates the generation of higher order modes to produce multimode interference, allowing high intensity modes to pass through the SMS while low intensity modes are filtered by the artificial SA. Following rounds of light transmission, low intensity modes are filtered and high intensity modes are locked in the cavity to generate mode-locked pulses. As shown in Fig. 5.2, a mode-locked pulse centred at 1567nm is successfully formed at threshold pump power of 189.2mW. The mode-locking operation is observable throughout the

pump power range of 189.2mW to 269.1mW. Additionally, the full width half maximum (FWHM) of optical spectrum is 0.2 nm.

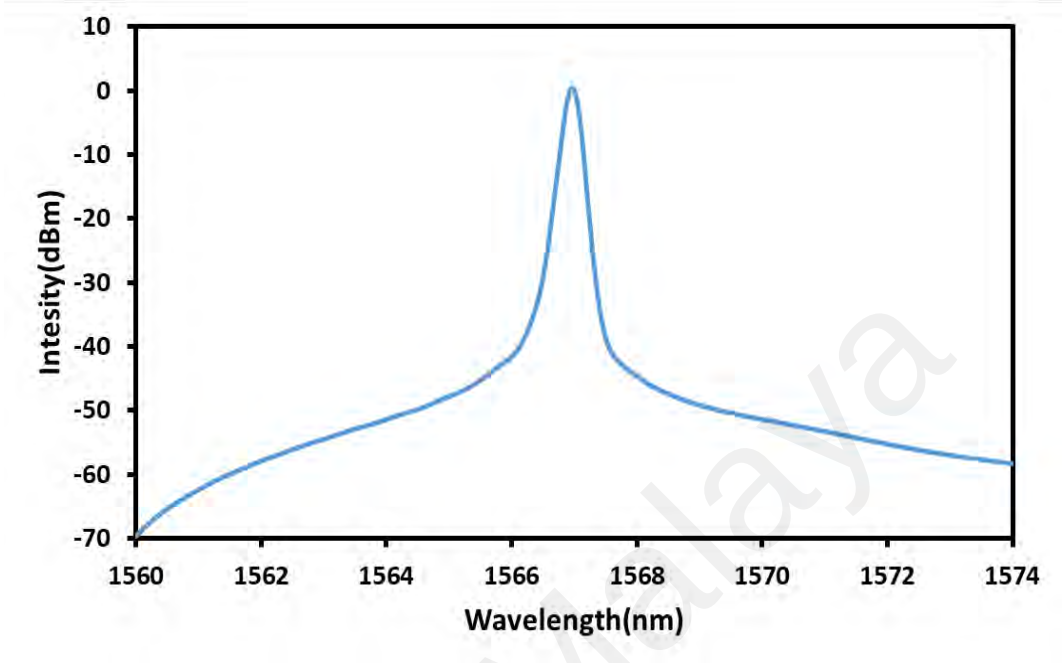

Figure 5.2: Optical spectrum of mode-locked EDFL at pump power of 189.2mW

Fig. 5.3 illustrates the mode-locked pulse train in the time domain. The pulse train oscillates stably in the EDFL with a peak-to-peak duration of 780ns, translating to a pulse repetition rate of 1.28MHz. The pulse width is 380 ns based on the oscilloscope reading. As demonstrated in Fig. 5.4, the average output power and average pulse energy are further investigated. Pump power is directly related to average output power and average pulse energy. With a pump power range of 189.2mW to 269.1mW, the average output power increases linearly ($R^2 = 0.99$) from 4.76mW to 7.68mW. In mode-locking operation, the laser efficiency is roughly 3.67%, which is close to prior reported lasers based on other SAs. Furthermore, the average pulse energy increases linearly with pump power, with the greatest pulse energy of 6.0nJ reported at a pump power of 269.1mW.

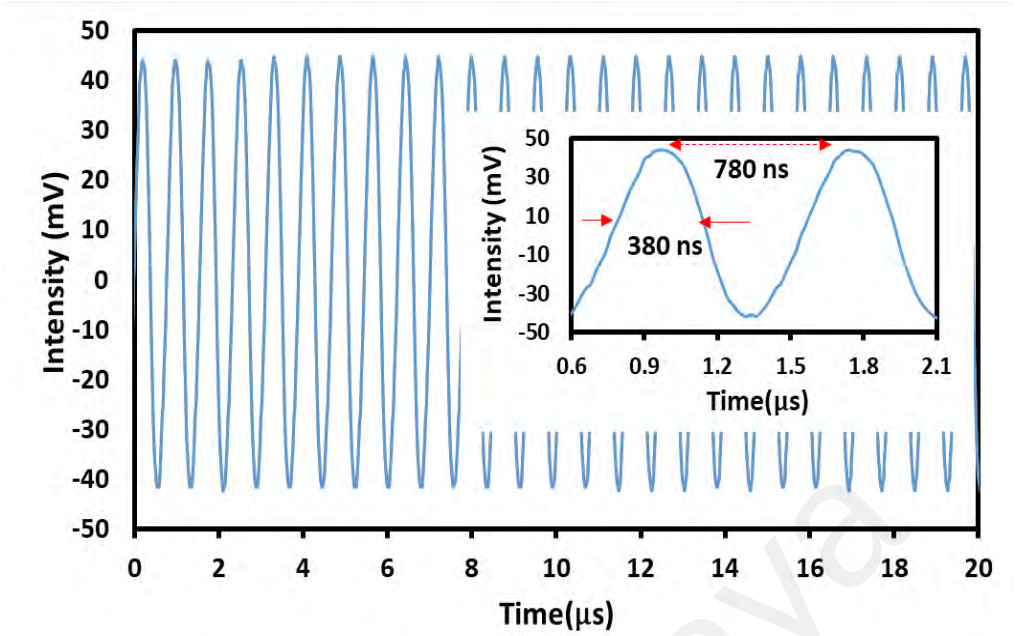

Figure 5.3: Typical pulse train of the mode-locked fiber laser and inset shows the enlarged two-pulse envelop

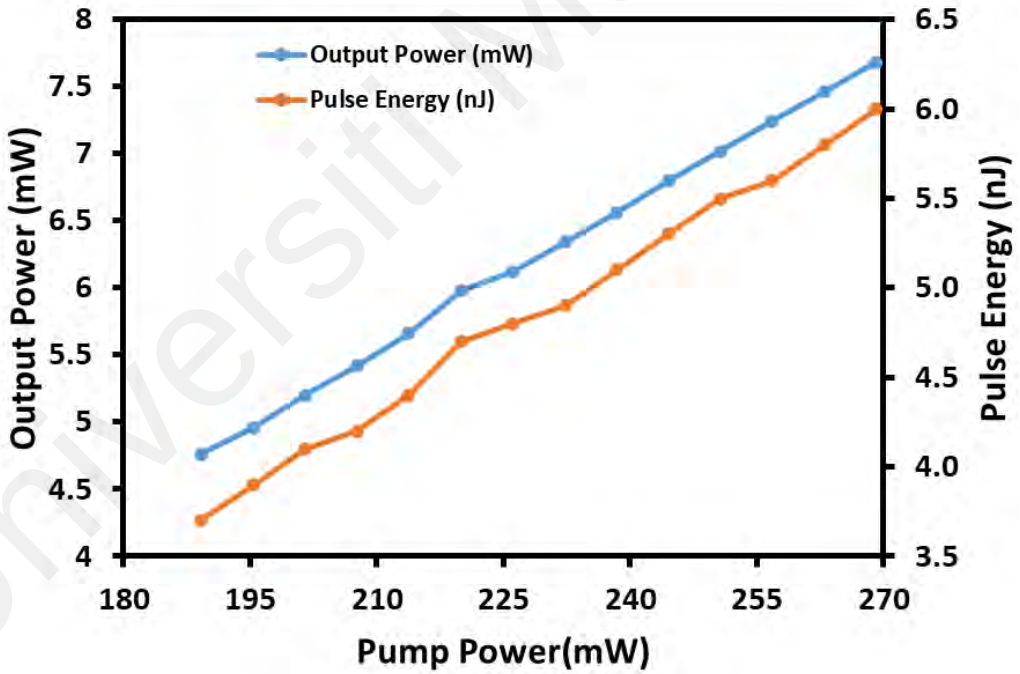

Figure 5.4: Average output power and pulse energy acquired from the mode-locked fiber laser with the variation of pump power

As illustrated in Fig. 5.5, the stability of the mode-locking operation caused by the SMS-based artificial SA is examined further. The frequency component has a signal-to-

noise ratio (SNR) of ~70dB and is situated at 1.28MHz. This implies that the mode-locked pulse train is being circulated in the ring fibre laser in a stable manner.

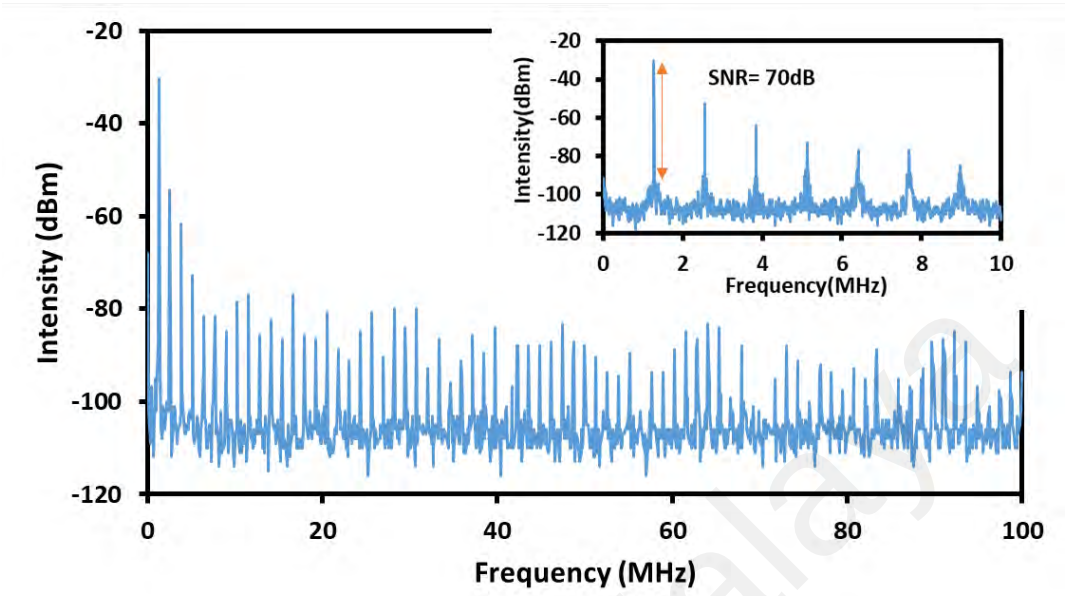

Figure 5.5: RF spectrum of the mode-locked fiber laser FBG

CHAPTER 6: CONCLUSION AND FUTURE WORKS

6.1 Conclusion

MRRs are frequently used in a variety of sectors of action, one of which is optical sensing. They can easily detect the surrounding media. The wide evanescent field of light promotes light interaction with the environmental medium, modifying the structure's resonance conditions. Singlemode-Multimode-Singlemode (SMS) sensors have gotten a lot of interest because of its ease of manufacture, capacity to sense different quantities, and higher sensitivity when compared to the most popular fiber optic sensor, Fiber Bragg Gratings (FBGs). In the meantime, several MF resonators and SMS interferometers have been employed to quantify numerous physical and chemical properties. However, fresh innovations and advances in this subject are continually being made. MRR and SMS devices are developed in this chapter, and their applications in sensing and fiber laser are discussed.

At first, the MRR was made up by intricately coiling the MF upon itself through the interplay of two surface forces: the Van der Waals force and electrostatic force. The comb propagation spectrum of the prepared MRR was acquired by using the ASE in tandem with OSA for two different samples with the loop diameters of approximately 285.6µm and 379.3µm. Both samples show an obvious resonant response with the smaller loop diameter indicating a better extinction ratio. On the other hand, the SMSF structure was built by directly splicing a 50 mm long MMF with two SMFs at both ends. The MMI effect within its structure was successfully demonstrated. Chapter 3 reported on the manufacture and description of both MRR and SMS devices.

The temperature and glycerin sensors were then reported in Chapter 4 using MRR and SMS device. The proposed sensors are simple and less complex since there is no involvement of any sensitive materials coated on it during the fabrication process. The

MRR sensor shows the resonant wavelength displacement of about 0.2 nm for every 5℃ increases of temperature. When the ambient temperature is varied between 55℃ and 75℃, the sensitivity of MRR is 0.18nm/℃ and the linearity is 0.8804. It was also observed that the transmitted light intensity of the MRR changes between -41.3 and -47.4 dBm, with a rate of 0.1587 dB/°C and a linearity of less than 10% when the ambient temperature changes from 55°C to 75°C. On the other hand, the MRR sensor also shows a significant wavelength and intensity modulation response to the change of concentrations of glycerin (propane-1,2,3-triol) in water. This is attributed to the change of cladding refractive index, which changes the phase and loss of the oscillating light inside the MRR structure. The sensor exhibits a sensitivity of 0.22nm/%Vol and -1.25 dB/%Vol as it was analyzed based on resonance wavelength shift and intensity modulation respectively.

The temperature and glycerin sensors were also realized by using a SMS structure as a probe. This sensor has significant wavelength and intensity modulation responses to changes in temperature and changes in glycerin (propane-1,2,3-triol) concentration in water. When the temperature gradually increases, the high-order modulus of MMF in the SMS structure will be affected. With a certain degree of excitation, the sensor sensitivities based on resonance wavelength shift and intensity modulation are -0.8nm/°C and 3.8605 dB/°C, respectively. When the concentration of the glycerin solution increases, the phase and loss of the oscillating light inside the SMS structure are changed due to changes in the RI of the cladding. The sensor sensitivity based on resonance wavelength shift is -1.152nm/%Vol.

The sensitivity of the two sensors to temperature change and the sensitivity of the liquid refractive index are summarized and compared, as shown in Table 6.1 and Table 6.2, the values shown in table are absolute values for numerical comparison.

Table 6.1: Comparation of Two Devices for Temperature Sensing Sensitivity

	MRR	SMS
Resonance Wavelength Shift	0.18nm/℃	0.80nm/℃
Intensity Modulation	0.1587dB/℃	3.8605dB/℃
Temperature Range: 55℃-75℃		

Table 6.2: Comparation of Two Devices for Liquid Refractive index Sensing Sensitivity

	MRR	SMS
Resonance Wavelength Shift	0.22nm/%Vol	1.152nm/%Vol
Intensity Modulation	1.25dB/%Vol	0.1144dB/%Vol
Glycerin Concentration Range: 20%Vol-60%Vol		

The range and unit of temperature and glycerin concentration are chosen in this research all based on the experimental conditions. The fiber core is made of silicon dioxide, its coefficient of thermal expansion is 0.5ppm/°C. Whereas cladding is usually made of gallium-doped silicon dioxide, which is approximately 11ppm/°C. In this paper, the thermal expansion factor with less influence is ignored because the temperature change experiment has more obvious damage to the MRR structure. Higher than 75℃,

the structure of MRR will be destroyed. The initial temperature of the temperature controller we used in this research is 50℃. Its minimal unit is 5℃. In the liquid refractive index experiment, the temperature is controlled, and there is no heating phenomenon when glycerin solution is in contact with fiber. The concentration selection of glycerin solution is also based on the same reason, the volume of pure glycerin in the solution accounted for more than 60%, the phenomenon of pure glycerin solution water absorption can not get the corresponding concentration of glycerin solution. The minimum interval unit of 10% is chosen because of the precision limitation of the deployment equipment. Through the above two tables, it can be seen that the SMS structure has higher sensitivity (larger value) in temperature change experiments, whether resonance wavelength shift or intensity modulation is used as the criterion of sensor sensitivity. In liquid refractive index sensing experiment, SMS structure is more sensitive based on resonance wavelength shift criterion. Under the criterion of intensity modulation, the MRR sensor is more sensitive. Since the experimental behaviour is destructive to the structure, each experiment can only be performed 1-2 times.

Finally, as detailed in Chapter 5, mode-locking functionality in EDFL was demonstrated utilising an SMS structure that operated as an artificial SA. The SMS-based SA successfully phase-locked the longitudinal modes oscillating in the EDFL cavity, resulting in mode-locked pulses at 1567 nm. The fundamental frequency of 1.28 MHz is used to calculate the pulse repetition rate. At a pump power of 269.1mW, the greatest average pulse energy obtained is 6.0nJ. The proposed artificial saturable absorber could help to build sustainable industry, innovation, and infrastructure.

6.2 Future Works

This experiment is only the basic experiment of MRR substance detection, and it can be seen that MRR has a great development future in substance detection. Through this experiment, it can be found that single-mode microfiber is not the best choice, because it is easy to break after stretching, and the structure is unstable after forming a ring. In addition, the use of flame heating to stretch the fiber will lead to uneven stretching, so the method of uniform stretching the fiber also has the prospect of improvement. In the process of precision optical experiments, the environment and system noise cannot be ignored. The control principle and the knowledge related to automation and computer field such as deep learning can be used to control, reduce, and eliminate most of the environmental impact in the experiment process, so as to obtain more accurate experimental results.

Due to the working principle of the mode-locked fiber laser itself, it needs SA to absorb and block the transmission of light in the fiber loop to a certain extent, so that it reaches saturation and then releases a higher energy pulse laser. By adjusting other components in the laser loop to suppress the multi-mode transmission of light in the MMF, all modes are closer to the same mode to enhance the interference effect, so as to obtain a more stable laser with a higher output energy.

REFERENCES

Agrawal, G. J. I. J. o. Q. E. (1984). Line narrowing in a single-mode injection laser due to external optical feedback. *20*(5), 468-471.

Ahuja, S. (2000). *Handbook of bioseparations*. Elsevier.

Ahuja, S., & Dong, M. (2005). *Handbook of pharmaceutical analysis by HPLC*. Elsevier.

Al-Bukhaiti, W. Q., Noman, A., Qasim, A. S., Al-Farga, A. J. I. J. o. A. I., & Research. (2017). Gas chromatography: Principles, advantages and applications in food analysis. *6*(1), 2319-1473.

Arévalo, F. J., Osuna-Sánchez, Y., Sandoval-Cortés, J., Di Tocco, A., Granero, A. M., Robledo, S. N., . . . Fernández, H. (2017). Development of an electrochemical sensor for the determination of glycerol based on glassy carbon electrodes modified with a copper oxide nanoparticles/multiwalled carbon nanotubes/pectin composite. *Sensors and Actuators B: Chemical*, *244*, 949-957. https://doi.org/10.1016/j.snb.2017.01.093

Armani, D., Kippenberg, T., Spillane, S., & Vahala, K. J. N. (2003). Ultra-high-Q toroid microcavity on a chip. *421*(6926), 925-928.

Asghari, A., Wang, C., Yoo, K. M., Rostamian, A., Xu, X., Shin, J.-D., . . . Chen, R. T. (2021). Fast, accurate, point-of-care COVID-19 pandemic diagnosis enabled through advanced lab-on-chip optical biosensors: Opportunities and challenges. *Applied physics reviews*, *8*(3).

Aslam, N., Zhou, H., Urbach, E. K., Turner, M. J., Walsworth, R. L., Lukin, M. D., & Park, H. (2023). Quantum sensors for biomedical applications. *Nature Reviews Physics*, *5*(3), 157-169.

Bilodeau, F., Hill, K., Faucher, S., & Johnson, D. J. J. o. L. T. (1988). Low-loss highly overcoupled fused couplers: Fabrication and sensitivity to external pressure. *6*(10), 1476-1482.

Birks, T. A., & Li, Y. W. J. J. o. L. T. (1992). The shape of fiber tapers. *10*(4), 432-438.

Bohren, C. F., & Huffman, D. R. (2008). *Absorption and scattering of light by small particles*. John Wiley & Sons.

Born, M., & Wolf, E. (2013). *Principles of optics: electromagnetic theory of propagation, interference and diffraction of light*. Elsevier.

Boucouvalas, A., & Georgiou, G. J. E. L. (1985). Biconical taper coaxial coupler filter. *22*(21), 1033-1034.

Brambilla, G., Xu, F., & Feng, X. J. E. L. (2006). Fabrication of optical fibre nanowires and their optical and mechanical characterisation. *42*(9), 1.

Brambilla, G. J. J. o. O. (2010). Optical fibre nanowires and microwires: a review. *12*(4), 043001.

Brambilla, G. J. O. F. T. (2010). Optical fibre nanotaper sensors. *16*(6), 331-342.

Calvo, M. L., & Lakshminarayanan, V. (2018). *Optical waveguides: from theory to applied technologies*. CRC press.

Canning, J., Srivastava, S. K., Peng, G., Verma, R., & Gupta, B. D. (2012). *Surface plasmon resonance based fiber optic glucose biosensor* Third Asia Pacific Optical Sensors Conference,

Cao, R., Yang, Y., Wang, M., Yi, X., Wu, J., Huang, S., & Chen, K. P. (2020). Multiplexable intrinsic Fabry–Perot interferometric fiber sensors for multipoint hydrogen gas monitoring. *Optics letters*, *45*(11), 3163-3166.

Chen, G., Zhang, Y., Huang, D., Zhang, X., Cao, H., & Chen, W. (2009). Photonic generation of a microwave signal by employing a microfiber ring resonator. *Optics Communications*, *282*(13), 2552-2555. https://doi.org/10.1016/j.optcom.2009.03.017

Chen, G. Y., Ding, M., Newson, T., & Brambilla, G. J. T. O. O. J. (2013). A review of microfiber and nanofiber based optical sensors. *7*(1).

Chen, W.-C., Li, P.-Y., Chou, C.-H., Chang, J.-L., & Zen, J.-M. (2015). A nonenzymatic approach for selective and sensitive determination of glycerol in biodiesel based on a PtRu-modified screen-printed edge band ultramicroelectrode. *Electrochimica Acta*, *153*, 295-299. https://doi.org/10.1016/j.electacta.2014.12.011

Chen, Y., Tiu, Z. C., Rosol, A. H. A., Tan, S. J., Dimyati, K., & Harun, S. W. (2024). All-fibre mode-locked laser using SMF-GIMF-SMF structure as artificial saturable absorber. *Results in Optics*, *14*. https://doi.org/10.1016/j.rio.2023.100603

Chung-Yen, C., & Guo, L. J. (2006). Design and optimization of microring resonators in biochemical sensing applications. *Journal of Lightwave Technology*, *24*(3), 1395-1402. https://doi.org/10.1109/jlt.2005.863333

Coillet, A., Cluzel, B., Vienne, G., Grelu, P., & de Fornel, F. J. A. P. B. (2010). Near-field characterization of glass microfibers on a low-index substrate. *101*, 291-295.

Corres, J. M., Arregui, F. J., & Matias, I. R. J. J. o. L. T. (2006). Design of humidity sensors based on tapered optical fibers. *24*(11), 4329-4336.

de Souza, F. C., de Vasconcellos Junior, F. J., Cabral, R. C., Fernández, T. L., & D'Elia, E. (2013). Simple enzymatic methods for glycerol analysis in commercial

beverages. *CyTA - Journal of Food*, *11*(3), 270-276. https://doi.org/10.1080/19476337.2012.732613

De Stefano, L., Moretti, L., Rendina, I., & Rotiroti, L. (2005). Pesticides detection in water and humic solutions using porous silicon technology. *Sensors and Actuators B: Chemical*, *111-112*, 522-525. https://doi.org/10.1016/j.snb.2005.03.047

Dimmick, T. E., Kakarantzas, G., Birks, T. A., & Russell, P. S. J. J. A. O. (1999). Carbon dioxide laser fabrication of fused-fiber couplers and tapers. *38*(33), 6845-6848.

Ding, Y., Yang, Q., Guo, X., Wang, S., Gu, F., Fu, J., . . . Tong, L. J. O. e. (2009). Nanowires/microfiber hybrid structure multicolor laser. *17*(24), 21813-21818.

Dong, M. W. (2006). *Modern HPLC for practicing scientists*. John Wiley & Sons.

Donlagi, D., & Culshaw, B. J. J. o. l. t. (2000). Propagation of the fundamental mode in curved graded index multimode fiber and its application in sensor systems. *18*(3), 334.

Đonlagić, D., & Završnik, M. J. O. l. (1997). Fiber-optic microbend sensor structure. *22*(11), 837-839.

Eftekhari, A. J. S., & Chemical, A. B. (2001). Glycerol biosensor based on glycerol dehydrogenase incorporated into polyaniline modified aluminum electrode using hexacyanoferrate as mediator. *80*(3), 283-289.

Eitenmiller, R. R., & Lee, J. (2004). *Vitamin E: food chemistry, composition, and analysis*. CRC Press.

Fang, Z., Chin, K., Qu, R., & Cai, H. (2012). *Fundamentals of optical fiber sensors* (Vol. 226). John Wiley & Sons.

Feng, C., Meng, L., Wang, H., Wang, D., Xu, Z., Wei, L., . . . Yuan, L. J. J. o. L. T. (2023). Multi-channel seven-core fiber SPR sensor without temperature and channel crosstalk.

Forouzeshfard, M. R., Ghafari, S., & Vafapour, Z. (2021). Solute concentration sensing in two aqueous solution using an optical metamaterial sensor. *Journal of Luminescence*, *230*. https://doi.org/10.1016/j.jlumin.2020.117734

Fu, B., Sun, J., Wang, C., Shang, C., Xu, L., Li, J., & Zhang, H. (2021). MXenes: Synthesis, optical properties, and applications in ultrafast photonics. *Small*, *17*(11), 2006054.

Fu, S., Sheng, Q., Zhu, X., Shi, W., Yao, J., Shi, G., . . . Peyghambarian, N. J. O. e. (2015). Passive Q-switching of an all-fiber laser induced by the Kerr effect of multimode interference. *23*(13), 17255-17262.

Fuentes-Fuentes, M. A., May-Arrioja, D. A., Guzman-Sepulveda, J. R., Torres-Cisneros, M., & Sánchez-Mondragón, J. J. J. S. (2015). Highly sensitive liquid core temperature sensor based on multimode interference effects. *15*(10), 26929-26939.

Gagliardi, R. M., & Karp, S. (1997). Optical Communication Technology and Application. In: Translated by Chen Genxiang, Beijing: Electronic Industries Publishing Company.

Gai, L., Li, J., & Zhao, Y. (2017). Preparation and application of microfiber resonant ring sensors: A review. *Optics & Laser Technology*, *89*, 126-136. https://doi.org/10.1016/j.optlastec.2016.10.002

Gao, J., Ning, T., Liu, Y., Shang, X., Han, X., Guo, Q., . . . Zhang, H. (2019). Generation of high-energy rectangular pulses in a nonlinear polarization rotation mode-locked ring fiber laser. *Applied optics*, *58*(28), 7897-7903.

Gaussoin, R. E., Berndt, W. L., Dockrell, C. A., Drijber, R. A. J. T. B., use,, & management. (2013). Characterization, development, and management of organic matter in turfgrass systems. *56*, 425-456.

Girault, P., Lorrain, N., Poffo, L., Guendouz, M., Lemaitre, J., Carré, C., . . . Vignaud, G. (2015). Integrated polymer micro-ring resonators for optical sensing applications. *Journal of applied Physics*, *117*(10), 104504.

Grob, R. L., & Barry, E. F. (2004). *Modern practice of gas chromatography*. John Wiley & Sons.

Guo, X., Li, Y., Jiang, X., & Tong, L. (2007). Demonstration of critical coupling in microfiber loops wrapped around a copper rod. *Applied Physics Letters*, *91*(7), 073512.

Guzmán-Sepúlveda, J. R., Guzmán-Cabrera, R., & Castillo-Guzmán, A. A. J. S. (2021). Optical sensing using fiber-optic multimode interference devices: a review of nonconventional sensing schemes. *21*(5), 1862.

Haris, H., Harun, S. W., Yupapin, P., Arof, H., & Apsari, R. (2020). Generation of Vector Soliton Pulses with Graphene Oxide Film in Mode-locked Erbium-doped Fiber Laser Cavity. *Nonlinear Optics Quantum Optics-Concepts in Modern Optics*, *52*(1-2), 111-118. <Go to ISI>://WOS:000509998200006

Harun, S. W., Lim, K., Tio, C., Dimyati, K., & Ahmad, H. J. O. (2013). Theoretical analysis and fabrication of tapered fiber. *124*(6), 538-543.

Higashihara, T., & Ueda, M. J. M. (2015). Recent progress in high refractive index polymers. *48*(7), 1915-1929.

Holloway, G., Maheswaran, R., Leeks, A., Bradby, S., & Wahab, S. (2010). Screening method for ethylene glycol and diethylene glycol in glycerin-containing products. *J Pharm Biomed Anal*, *51*(3), 507-511. https://doi.org/10.1016/j.jpba.2009.08.025

Hossain, M. S., Sen, S., & Hossain, M. M. J. P. S. (2021). Performance analysis of octagonal photonic crystal fiber (O-PCF) for various communication applications. *96*(5), 055506.

Ippen, E., Shank, C., & Dienes, A. (1972). Passive mode locking of the cw dye laser. *Applied Physics Letters*, *21*(8), 348-350.

Irawati, N., Hatta, A. M., Yhuwana, Y. G. Y., & Sekartedjo. (2019). Heart Rate Monitoring Sensor Based on Singlemode-Multimode-Singlemode Fiber. *Photonic Sensors*, *10*(2), 186-193. https://doi.org/10.1007/s13320-019-0572-7

Jha, R., Villatoro, J., Badenes, G., & Pruneri, V. J. O. L. (2009). Refractometry based on a photonic crystal fiber interferometer. *34*(5), 617-619.

Jiang, X., Tong, L., Vienne, G., Guo, X., Tsao, A., Yang, Q., & Yang, D. (2006). Demonstration of optical microfiber knot resonators. *Applied Physics Letters*, *88*(22). https://doi.org/10.1063/1.2207986

Jin, H. L. (2013). Investigated Solution Concentration Sensor with the Single Mode-Multimode-FBG. *Applied Mechanics and Materials*, *433-435*, 237-240. https://doi.org/10.4028/www.scientific.net/AMM.433-435.237

Jungermann, E., & Sonntag, N. O. (2018). *Glycerine: a key cosmetic ingredient*. Routledge.

Kakarantzas, G., Dimmick, T., Birks, T., Le Roux, R., & Russell, P. S. J. J. O. L. (2001). Miniature all-fiber devices based on CO 2 laser microstructuring of tapered fibers. *26*(15), 1137-1139.

Kienhuis, A. S., Soeteman-Hernandez, L. G., Bos, P. M., Cremers, H. W., Klerx, W. N., & Talhout, R. J. T. I. D. (2015). Potential harmful health effects of inhaling nicotine-free shisha-pen vapor: a chemical risk assessment of the main components propylene glycol and glycerol. *13*, 1-6.

Kieu, K. Q., & Mansuripur, M. J. I. p. t. l. (2006). Biconical fiber taper sensors. *18*(21), 2239-2241.

Kumar, S., & Singh, R. (2021). Recent optical sensing technologies for the detection of various biomolecules. *Optics & Laser Technology*, *134*, 106620.

Lam, D., & Garside, B. K. J. A. o. (1981). Characterization of single-mode optical fiber filters. *20*(3), 440-445.

Le Kien, F., Balykin, V., & Hakuta, K. J. P. R. A. (2006). Angular momentum of light in an optical nanofiber. *73*(5), 053823.

Lee, B. H., Kim, Y. H., Park, K. S., Eom, J. B., Kim, M. J., Rho, B. S., & Choi, H. Y. (2012). Interferometric fiber optic sensors. *Sensors*, *12*(3), 2467-2486.

Lee, J., & Kim, D. J. O. e. (2006). Determination of the differential mode delay of a multimode fiber using Fourier-domain intermodal interference analysis. *14*(20), 9016-9021.

Li, E., Wang, X., & Zhang, C. J. A. p. l. (2006). Fiber-optic temperature sensor based on interference of selective higher-order modes. *89*(9).

Li, E. J. I. P. T. L. (2007). Sensitivity-enhanced fiber-optic strain sensor based on interference of higher order modes in circular fibers. *19*(16), 1266-1268.

Li, E. J. O. l. (2007). Temperature compensation of multimode-interference-based fiber devices. *32*(14), 2064-2066.

Li, J., Li, Z., Yang, J., Zhang, Y., & Ren, C. (2020). High sensitivity temperature probe based on elliptical microfiber knot ring. *Results in Physics*, *16*. https://doi.org/10.1016/j.rinp.2020.102953

Li, J., Zhang, Z., Sun, Z., Luo, H., Liu, Y., Yan, Z., . . . Turitsyn, S. K. (2014). All-fiber passively mode-locked Tm-doped NOLM-based oscillator operating at 2-μm in both soliton and noisy-pulse regimes. *Optics express*, *22*(7), 7875-7882.

Li, L., Pang, L., Wang, R., Zhang, X., Hui, Z., Han, D., . . . Liu, W. (2022). Ternary transition metal dichalcogenides for high power vector dissipative soliton ultrafast fiber laser. *Laser & Photonics Reviews*, *16*(2), 2100255.

Li, N., Zhou, Q., Li, X., Chu, W., Adkins, J., & Zheng, J. (2014). Electrochemical detection of free glycerol in biodiesel using electrodes with single gold particles in highly ordered SiO2 cavities. *Sensors and Actuators B: Chemical*, *196*, 314-320. https://doi.org/10.1016/j.snb.2014.02.017

Li, X., Chen, N., Zhou, X., Gong, P., Wang, S., Zhang, Y., & Zhao, Y. (2021). A review of specialty fiber biosensors based on interferometer configuration. *Journal of Biophotonics*, *14*(6), e202100068.

Lim, K., Harun, S., Arof, H., & Ahmad, H. (2012a). Fabrication and applications of microfiber. *Selected Topics on Optical Fiber Technology*, 473-508.

Lim, K., Harun, S., Arof, H., & Ahmad, H. J. S. T. o. O. F. T. (2012b). Fabrication and applications of microfiber. 473-508.

Liu, Z., Li, G., Zhang, A., Zhou, G., & Huang, X. (2021). Ultra-sensitive optical fiber sensor based on intermodal interference and temperature calibration for trace detection of copper (II) ions. *Opt Express*, *29*(15), 22992-23005. https://doi.org/10.1364/OE.434687

Lou, J., Wang, Y., & Tong, L. J. S. (2014). Microfiber optical sensors: A review. *14*(4), 5823-5844.

Lukose, J., Chidangil, S., & George, S. D. (2021). Optical technologies for the detection of viruses like COVID-19: Progress and prospects. *Biosensors and Bioelectronics*, *178*, 113004.

Luo, J., Wang, H., Cai, X., Luo, Z., & Fu, H. (2023). Temperature-sensing scheme based on a passively mode-locked fiber laser via beat frequency demodulation. *Chinese Optics Letters*, *21*(2). https://doi.org/10.3788/col202321.020603

Luo, X., Li, Y. J. J. o. P., & Environment, t. (2014). Synthesis and characterization of polyols and polyurethane foams from PET waste and crude glycerol. *22*, 318-328.

Lv, H., Zhang, K., Ma, X., Zhong, W., Wang, Y., & Gao, X. J. P. O. (2021). Optimum design of the surface plasmon resonance sensor based on polymethyl methacrylate fiber. *6*, 100054.

Ma, Q., Ren, G., Xu, K., & Ou, J. Z. (2021). Tunable optical properties of 2D materials and their applications. *Advanced Optical Materials*, *9*(2), 2001313.

Mary, R., Choudhury, D., & Kar, A. K. (2014). Applications of fiber lasers for the development of compact photonic devices. *IEEE Journal of Selected Topics in Quantum Electronics*, *20*(5), 72-84.

Mehta, A., Mohammed, W., & Johnson, E. G. J. I. P. T. L. (2003). Multimode interference-based fiber-optic displacement sensor. *15*(8), 1129-1131.

Mohammed, W. S., Mehta, A., & Johnson, E. G. J. J. o. L. T. (2004). Wavelength tunable fiber lens based on multimode interference. *22*(2), 469.

Mohammed, W. S., Smith, P. W., & Gu, X. J. O. l. (2006). All-fiber multimode interference bandpass filter. *31*(17), 2547-2549.

Mondal, S., Ganguly, R., & Mondal, K. (2021). Topological Insulators: An In-Depth Review of Their Use in Modelocked Fiber Lasers. *Annalen der Physik*, *533*(6), 2000564.

Motia, S., Bouchikhi, B., Llobet, E., & El Bari, N. (2020). Synthesis and characterization of a highly sensitive and selective electrochemical sensor based on molecularly imprinted polymer with gold nanoparticles modified screen-printed electrode for glycerol determination in wastewater. *Talanta*, *216*, 120953. https://doi.org/10.1016/j.talanta.2020.120953

Mu, G., Liu, Y., Qin, Q., Tan, Z., Li, G., Wang, M., & Yan, F. J. I. P. T. L. (2020). Refractive index sensing based on the analysis of D-shaped multimode fiber specklegrams. *32*(8), 485-488.

Niessen, W. M. (2006). *Liquid chromatography-mass spectrometry*. CRC press.

Okamoto, K. (2021). *Fundamentals of optical waveguides*. Elsevier.

Paiva, V. M., Assis, K. L. d. S. C., Archanjo, B. S., Ferreira, D. R., Senna, C. A., Ribeiro, E. S., . . . D'Elia, E. (2021). Electrochemical Analysis of Free Glycerol in Biodiesel Using Reduced Graphene Oxide and Gold/Palladium Core-Shell Nanoparticles Modified Glassy Carbon Electrode. *Processes*, *9*(8). https://doi.org/10.3390/pr9081389

Pang, L., Zhao, M., Zhao, Q., Li, L., Wang, R., Wu, R., . . . Liu, W. (2022). GaSb Film is a Saturable Absorber for Dissipative Soliton Generation in a Fiber Laser. *ACS applied materials & interfaces*.

Pharmacopoeia, E. (2014). European directorate for the quality of medicines & healthcare (EDQM). In: Strasbourg France.

Pierce, M. C., Jackson, S. D., Golding, P. S., Dickinson, B., Dickinson, M. R., King, T. A., & Sloan, P. (2001). Development and application of fiber lasers for medical applications. Optical Fibers and Sensors for Medical Applications,

Poblete-Castro, I., Wittmann, C., & Nikel, P. I. J. M. B. (2020). Biochemistry, genetics and biotechnology of glycerol utilization in Pseudomonas species. *13*(1), 32-53.

Pragst, F. (2008). High performance liquid chromatography in forensic toxicological analysis. In *Handbook of Analytical Separations* (Vol. 6, pp. 447-489). Elsevier.

Presti, D. L., Massaroni, C., Zaltieri, M., Sabbadini, R., Carnevale, A., Di Tocco, J., . . . Schena, E. (2020). A Magnetic Resonance-compatible wearable device based on functionalized fiber optic sensor for respiratory monitoring. *IEEE Sensors Journal*, *21*(13), 14418-14425.

Rajan, G. (2017). *Optical fiber sensors: advanced techniques and applications*. CRC press.

Rao, Y.-J. (2006). Recent progress in fiber-optic extrinsic Fabry–Perot interferometric sensors. *Optical Fiber Technology*, *12*(3), 227-237.

Reyes-Vera, E., Cordeiro, C. M., & Torres, P. (2017). Highly sensitive temperature sensor using a Sagnac loop interferometer based on a side-hole photonic crystal fiber filled with metal. *Applied optics*, *56*(2), 156-162.

Ribeiro, R., Werneck, M. J. S., & Physical, A. A. (2004). An intrinsic graded-index multimode optical fibre strain-gauge. *111*(2-3), 210-215.

Ridho, M. R., Sari, D. N., Prasintha, P., Fikroh, U. Z., Yasin, M., Trilaksana, H., & Samian. (2020). Liquid level sensor using U-bent SMS fiber structure. AIP Conference Proceedings,

Rowe, R. C., Sheskey, P., & Quinn, M. (2009). *Handbook of pharmaceutical excipients*. Libros Digitales-Pharmaceutical Press.

Sahota, J. K., Gupta, N., & Dhawan, D. (2020a). Fiber Bragg grating sensors for monitoring of physical parameters: A comprehensive review. *Optical Engineering*, *59*(6), 060901.

Sahota, J. K., Gupta, N., & Dhawan, D. (2020b). Fiber Bragg grating sensors for monitoring of physical parameters: A comprehensive review. *Optical Engineering*, *59*(6), 060901-060901.

Samsamnun, F. S. M., Zulkipli, N. F., Majid, W. H. A., Khudus, M., Shuhaimi, A., Rosol, A. H. A., . . . Harun, S. W. (2020). MEH-PPV organic material as saturable absorber for Q-switching and mode-locking applications. *Journal of Modern Optics*, *67*(8), 746-753. https://doi.org/10.1080/09500340.2020.1769762

Sedghi, R., Shahbeik, H., Rastegari, H., Rafiee, S., Peng, W., Nizami, A.-S., . . . Aghbashlo, M. (2022). Turning biodiesel glycerol into oxygenated fuel additives and their effects on the behavior of internal combustion engines: A comprehensive systematic review. *Renewable and Sustainable Energy Reviews*, *167*. https://doi.org/10.1016/j.rser.2022.112805

Shao, L.-Y., Zhang, A. P., Liu, W.-S., Fu, H.-Y., & He, S. J. I. P. T. L. (2007). Optical refractive-index sensor based on dual fiber-Bragg gratings interposed with a multimode-fiber taper. *19*(1), 30-32.

Shi, L., Xu, Y., Tan, W., & Chen, X. J. S. (2007). Simulation of optical microfiber loop resonators for ambient refractive index sensing. *7*(5), 689-696.

Shi, W., Fang, Q., Zhu, X., Norwood, R. A., & Peyghambarian, N. (2014). Fiber lasers and their applications. *Applied optics*, *53*(28), 6554-6568.

Shiner, B. (2016). Fiber lasers continue to gain market share in material processing applications. *Manuf. Eng.*, *156*, 79-85.

Silva, S., Frazão, O., Santos, J., Malcata, F. J. S., & Chemical, A. B. (2012). A reflective optical fiber refractometer based on multimode interference. *161*(1), 88-92.

Skoog, D. A., Holler, F. J., & Crouch, S. R. (2017). *Principles of instrumental analysis*. Cengage learning.

Skoog, D. A., West, D. M., Holler, F. J., & Crouch, S. R. (2013). *Fundamentals of analytical chemistry*. Cengage learning.

Smith, C., Gisser, D., Young, M., & Powers Jr, S. J. A. P. L. (1974). Liquid-crystal optical activity for temperature sensing. *24*(10), 453-454.

Snyder, L. R., Kirkland, J. J., & Dolan, J. W. (2011). *Introduction to modern liquid chromatography*. John Wiley & Sons.

Snyder, L. R., Kirkland, J. J., & Dolan, J. W. J. I., Hobeken, New Yersey, Canada. (2010). Introduction to modern liquid chromatography John Wiley & Sons. 202.

Soldano, L. B., & Pennings, E. C. (1995). Optical multi-mode interference devices based on self-imaging: principles and applications. *Journal of Lightwave Technology*, *13*(4), 615-627.

Soldano, L. B., & Pennings, E. C. J. J. o. l. t. (1995). Optical multi-mode interference devices based on self-imaging: principles and applications. *13*(4), 615-627.

Su, H., & Huang, X. G. (2007). Fresnel-reflection-based fiber sensor for on-line measurement of solute concentration in solutions. *Sensors and Actuators B: Chemical*, *126*(2), 579-582. https://doi.org/10.1016/j.snb.2007.04.008

Su, Y., Lan, Z., Wang, J., Zeng, L., Zhou, D., Peng, Z., . . . Liu, Y. (2021). Optical Fiber Sensor for Determination of Methanol Ratio in Methanol-Doped Ethanol Based on Two Cholesteric Liquid Crystal Droplets Embedded in Chitosan. *Journal of Lightwave Technology*, *39*(15), 5170-5176. https://doi.org/10.1109/jlt.2021.3078744

Sumetsky, M., Dulashko, Y., Fini, J., Hale, A., & DiGiovanni, D. (2006). The microfiber loop resonator: theory, experiment, and application. *Journal of Lightwave Technology*, *24*(1), 242-250.

Sumetsky, M., Dulashko, Y., Fini, J. M., Hale, A., & DiGiovanni, D. J. (2006). The microfiber loop resonator: theory, experiment, and application. *Journal of Lightwave Technology*, *24*(1), 242-250. https://doi.org/10.1109/jlt.2005.861127

Syuhada, A., Shamsudin, M. S., Daud, S., Krishnan, G., Harun, S. W., & Aziz, M. S. A. (2021). Single-mode modified tapered fiber structure functionalized with GO-PVA composite layer for relative humidity sensing. *Photonic Sensors*, *11*, 314-324.

Tang, J., Zhou, J., Guan, J., Long, S., Yu, J., Guan, H., . . . Chen, Z. (2017). Fabrication of Side-Polished Single Mode-Multimode-Single Mode Fiber and Its Characteristics of Refractive Index Sensing. *IEEE Journal of Selected Topics in Quantum Electronics*, *23*(2), 238-245. https://doi.org/10.1109/jstqe.2016.2615941

Taya, S. A., Sharma, A., Doghmosh, N., & Colak, I. (2022). Detection of water concentration in ethanol solution using a ternary photonic crystal-based sensor. *Materials Chemistry and Physics*, *279*. https://doi.org/10.1016/j.matchemphys.2022.125772

Tong, L., Hu, L., Zhang, J., Qiu, J., Yang, Q., Lou, J., . . . Ye, Z. J. O. E. (2006). Photonic nanowires directly drawn from bulk glasses. *14*(1), 82-87.

Tong, L., Lou, J., & Mazur, E. J. O. E. (2004). Single-mode guiding properties of subwavelength-diameter silica and silicon wire waveguides. *12*(6), 1025-1035.

Tong, L., Lou, J., Ye, Z., Svacha, G. T., & Mazur, E. J. N. (2005). Self-modulated taper drawing of silica nanowires. *16*(9), 1445.

Tripathi, S. M., Kumar, A., Varshney, R. K., Kumar, Y. B. P., Marin, E., & Meunier, J. P. (2009). Strain and Temperature Sensing Characteristics of Single-Mode–Multimode–Single-Mode Structures. *Journal of Lightwave Technology*, *27*(13), 2348-2356. https://doi.org/10.1109/jlt.2008.2008820

Vollmer, F., & Yang, L. (2012). Review Label-free detection with high-Q microcavities: a review of biosensing mechanisms for integrated devices. *Nanophotonics*, *1*(3-4), 267-291.

Wan, B.-F., Wang, Q.-Y., Peng, H.-M., Ye, H.-N., & Zhang, H.-F. (2021). A Late-Model Optical Biochemical Sensor Based on OTS for Methane Gas and Glucose Solution Concentration Detection. *IEEE sensors journal*, *21*(19), 21465-21472. https://doi.org/10.1109/jsen.2021.3103548

Wang, P., Zhang, S., Wang, R., Farrell, G., Zhang, M., Geng, T., . . . Tian, K. (2019). Temperature-insensitive refractometer based on an RI-modulated singlemode-multimode-singlemode fibre structure. *Opt Express*, *27*(10), 13754-13764. https://doi.org/10.1364/OE.27.013754

Wang, Q., Farrell, G., & Yan, W. (2008a). Investigation on Single-Mode–Multimode–Single-Mode Fiber Structure. *Journal of Lightwave Technology*, *26*(5), 512-519. https://doi.org/10.1109/jlt.2007.915205

Wang, Q., Farrell, G., & Yan, W. (2008b). Investigation on single-mode–multimode–single-mode fiber structure. *Journal of Lightwave Technology*, *26*(5), 512-519.

Wang, Q., Farrell, G., & Yan, W. J. J. o. L. T. (2008c). Investigation on single-mode–multimode–single-mode fiber structure. *26*(5), 512-519.

Wang, Q., & Farrell, G. J. O. l. (2006). All-fiber multimode-interference-based refractometer sensor: proposal and design. *31*(3), 317-319.

Wang, W., Mai, Z., Chen, Y., Wang, J., Li, L., Su, Q., . . . Hong, X. (2017). A label-free fiber optic SPR biosensor for specific detection of C-reactive protein. *Scientific reports*, *7*(1), 16904.

Wang, X., Lewis, E., & Wang, P. (2017). Investigation of the self-imaging position of a singlemode-multimode-singlemode optical fiber structure. *Microwave and Optical Technology Letters*, *59*(7), 1645-1651. https://doi.org/10.1002/mop.30605

Watson, D. G. (2020). *Pharmaceutical analysis E-book: a textbook for pharmacy students and pharmaceutical chemists*. Elsevier Health Sciences.

Williams, M., Todd, G. D., Roney, N., Crawford, J., Coles, C., McClure, P. R., . . . Citra, M. (2013). Toxicological profile for manganese.

Wu, X., & Tong, L. (2013). Optical microfibers and nanofibers. Nanophotonics 2 (5–6): 407–428. In.

Xu, F., & Brambilla, G. (2007). Manufacture of 3-D Microfiber Coil Resonators. *IEEE Photonics Technology Letters*, *19*(19), 1481-1483. https://doi.org/10.1109/lpt.2007.903762

Xu, N., Sun, S., Shang, X., Zhang, H., & Li, D. (2022). Harmonic and fundamental-frequency mode-locked operations in an Er-doped fiber laser using a Cr 2 Si 2 Te 6-based saturable absorber. *Optical Materials Express*, *12*(1), 166-173.

Xu, Y., Ren, L., Liang, J., Ma, C., Wang, Y., Chen, N., & Qu, E. (2014). A simple, polymer-microfiber-assisted approach to fabricating the silica microfiber knot resonator. *Optics Communications*, *321*, 157-161. https://doi.org/10.1016/j.optcom.2014.01.077

Yang, Y., Jiang, F., Zeng, Q., Wang, K., Wang, Z., & Song, Y. (2023). Thulium-doped multi-wavelength and mode-locked fiber laser based on multimode interference. *Infrared Physics & Technology*, *133*. https://doi.org/10.1016/j.infrared.2023.104869

Yipeng, L., Xin, W., Hongjuan, Y., Shanshan, W., & Jing, W. (2015). Resonant Mode Characteristics of Microfiber Knot-Type Ring Resonator and Its Salinity Sensing Experiment. *IEEE Photonics Journal*, *7*(4), 1-8. https://doi.org/10.1109/jphot.2015.2450533

Yu, H., Xiong, L., Chen, Z., Li, Q., Yi, X., Ding, Y., . . . Ding, Y. (2014). Solution concentration and refractive index sensing based on polymer microfiber knot resonator. *Applied Physics Express*, *7*(2). https://doi.org/10.7567/apex.7.022501

Yu, Y., Teng, H., Wang, H., Wang, L., Zhu, J., Fang, S., . . . Wei, Z. (2018). Highly-stable mode-locked PM Yb-fiber laser with 10 nJ in 93-fs at 6 MHz using NALM. *Optics express*, *26*(8), 10428-10434.

Zain, H. A., Jali, M. H., Rahim, H. R. A., Johari, M. A. M., Yusof, H. H. M., Thokchom, S., . . . Harun, S. W. (2020). ZnO nanorods coated microfiber loop resonator for relative humidity sensing. *Optical Fiber Technology*, *54*, 102080.

Zeb, K., Lu, Z., Liu, J., Mao, Y., Liu, G., Poole, P. J., . . . Jiang, W. J. O. E. (2021). InAs/InP quantum dash buried heterostructure mode-locked laser for high capacity fiber-wireless integrated 5G new radio fronthaul systems. *29*(11), 16164-16174.

Zhang, H., Jin, L., Zhang, H., Xu, Y., Shi, L., Wang, T., . . . Wang, D. J. O. C. (2019). All-fiber nonlinear optical switch based on polarization controller coiled SMF–GIMF–SMF for ultrashort pulse generation. *452*, 7-11.

Zhang, X., Li, L., Zou, X., Luo, B., Pan, W., Yan, L., & Wu, Q. (2020). Angled fiber-based Fabry–Perot interferometer. *Optics letters*, *45*(2), 292-295.

Zhang, X., Xing, X., Li, J., Peng, X., Qiao, L., Liu, Y., . . . Xiao, W. J. A. P. L. (2022). Controllable epitaxy of quasi-one-dimensional topological insulator α-Bi4Br4 for the application of saturable absorber. *120*(9).

Zhang, Y., Zhang, X., Zhang, F., Wu, J., Wang, G., & Shum, P. P. (2011). Photonic generation of millimeter-wave ultra-wideband signal using microfiber ring resonator. *Optics Communications*, *284*(7), 1803-1806. https://doi.org/10.1016/j.optcom.2010.09.091

Zhao, C., Qiu, H., Chen, H., Hu, X., Yu, Q., Lian, Z., . . . Physical, A. A. (2021). In-fiber Mach-Zehnder temperature sensor using silicone-oil-filled dual core fiber. *323*, 112644.